5-2017

Multifunctional Reconfigurable Antennas and Arrays Operating at 60 GHz band

Abdurazag Mohamed Khalat
Utah State University

MULTIFUNCTIONAL RECONFIGURABLE ANTENNAS AND ARRAYS

OPERATING AT 60 GHZ BAND

by

Abdurazag Mohamed Khalat

A dissertation submitted in partial fulfillment
of the requirements for the degree

of

DOCTOR OF PHILOSOPHY

in

Electrical Engineering

Approved:

Bedri A. Cetiner, Ph.D. Major Professor	Doran J. Baker, Ph.D. Committee Member
Jacob Gunther, Ph.D. Committee Member	Reyhan Baktur, Ph.D. Committee Member
T.C. Shen, Ph.D. Committee Member	Mark R. McLellan, Ph.D. Vice President for Research and Dean of the School of Graduate Studies

UTAH STATE UNIVERSITY
Logan, Utah

2017

ABSTRACT

Multifunctional Reconfigurable Antennas and Arrays Operating at 60 GHz band

by

Abdurazag Mohamed Khalat, Doctor of Philosophy

Utah State University, 2017

Major Professor: Bedri A. Cetiner, Ph.D.
Department: Electrical and Computer Engineering

To meet the ever increasing demand of high data rate, millimeter-wave (mm-wave) wireless communication has become an area of intense research due to the capability of offering very broad bandwidth. However, the propagation losses increase as a function of operation frequency. Therefore, there is need for antenna systems with high gain and beam-steering capability at elevated frequencies, which comes at the expense of high cost and increased complexity. This dissertation demonstrates the design, micro-fabrication, and characterization of two different antennas and two different antenna arrays. A broadband patch antenna operating within $(57-66)$ GHz band, which works as a building block to create a multifunctional reconfigurable antenna (MRA) that is capable of beam steering in three directions pertaining to $\theta \in \{-30^0, 0^0, 30^0\}$; $\phi = 90^0$. These standalone antennas were then put in a linear formation to create a 2×8 planar array and a 4×1 multifunctional reconfigurable antenna array (MRAA) to increase the gain further and to offer wider bandwidth. The proposed novel MRA and MRAA possess variable element factors, which potentially can feature as the main building blocks of mm-wave reconfigurable wireless communication systems with reduced cost and complexity.

(71 pages)

PUBLIC ABSTRACT

Multifunctional Reconfigurable Antennas and Arrays Operating at 60 GHz band

Abdurazag Mohamed Khalat

In this digital era, the demand for faster, reliable, and adaptive wireless communication systems is increasing. Various factors can affect the signal propagation in the wireless medium, such as weather, broadcast environment, physical obstructions, etc. This study aims to improve the antenna performance by means of dynamically altering its properties so that it can adapt to different environments and communication scenarios. This study is not resorting in a traditional antenna design, but rather explores an alternative approach known as the multifunctional reconfigurable antennas (MRAs). Unlike its predecessor, i.e., legacy antennas, MRAs can dynamically change its operation frequency, radiation pattern, and polarization, which makes it an alternative technology toolbox for next-generation wireless communication systems. Design, micro-fabrication, and characterization of two standalone antennas and two antenna arrays are presented in this dissertation. These antennas are capable of operating within the entire IEEE 802.11ad (WiGig) band. The first design is a broadband patch antenna operating at $(57 - 66)$ GHz. The second design is an MRA which provides three distinct beam directions pertaining to: $\theta \in \{-30^0, 0^0, 30^0\}$; $\phi = 90^0$. The third design is a 2×8 patch multifunctional reconfigurable antenna array (MRAA) which operates within the frequency band of (57- 66) GHz an extension of the first design. Last, the fourth design is an MRAA with three parasitic layers; an extension of the second design. Finally, this dissertation concludes with plans for future work, which proposes the development of MRAs and MRAAs with dual-frequency operation.

Dedicated to my wife and our children!

ACKNOWLEDGMENTS

I would like to express my highest regards and gratitude to my advisor and mentor, Dr. Bedri A. Cetiner, who not only gave me the required knowledge to pursue my research through the subjects he taught, but also always gave the required moral support during my hard times, as well as encouraged my presentation skills on a regular basis.

I would like to thank my committee members, Dr. Doran Baker, Dr. Jacob Gunther, Dr. Reyhan Baktur, and Dr. T.C. Shen, who extended their support.

I would like to thank all my friends. I never felt lonely or dejected, and their endless support is the reason that kept me moving forward during difficult times of graduate studies.

I would also like to thank my wife and her family for having taken care of me in hard times. Finally, the constant love and affection from my family is the backbone of any successful endeavor in my life. Without their constant support and encouragement for quality education I would never have achieved the right kind of exposure to fulfill my dream of working in my area of interest.

Abdurazag Khalat

CONTENTS

LIST OF TABLES

LIST OF FIGURES

ACRONYMS

3-D	Three-Dimensional
BCB	Benzocyclobutene
BW	Bandwidth
CB	Conductor-Backed
Cr	Chromium
CPW	Coplanar Wave Guide
Cu	Copper
DI	Distilled Water
EM	Electro Magnetic
FCC	Federal Communication Commission
GHz	Giga Hertz
HFSS	High Frequency Structure Simulator
HMDS	Hexamethylisilazazne
IOT	Internet of Thing
LOS	Line of Sight
LTCC	Low Temperature Co-fired Ceramic
NLOS	Non-Line of Sight
MEMS	Micro Electro Mechanical Systems
MHz	Mega Hertz
MRA	Multifunctional Reconfigurable Antenna
PCB	Printed Circuit Board
PR	Photo-Resistor
RF	Radio Frequency
UV	Ultra Violet
VO_2	Vanadium Oxide
VSWR	Voltage Standing Wave Ratio
WiGig	Wireless Gigabit

CHAPTER 1

INTRODUCTION

The demand of high data rate has been increasing exponentially in recent years due to the expansion of smart hand-held devices, device to device communication and cloud-based applications. New concepts like Internet of Things (IoT), Vehicular Ad-Hoc Network (VANET), Machine to Machine Communication (M2M) are adding more overhead to the already expanding demand. However, the capacity of wireless communication depends on its spectral efficiency and bandwidth. At present, the physical technologies are already operating at the boundary of Shannon capacity. It is the communication channel bandwidth that remains largely unexploited. Currently almost all the wireless communication systems use the "beachfront spectrum" [1], i.e., 300 MHz to 3 GHz frequency band. The future 5G network is expected to have a paradigm shift to mm-wave band ranging from 3 GHz to 300 GHz [2] because of the availability of an extremely large unutilized bandwidth at this spectrum. Recently the Federal Communications Commission (FCC) has opened the spectrum between 59-64 GHz for unlicensed wireless communication. In response, the development of wireless communication systems operating at higher frequencies (WiGig, 60 GHz) has become a popular research area of interest for both academy and industry [3–7]. Additionally, the future wireless systems are envisaged to enable wireless connectivity for everybody. The requirements for these systems are reduced weight/size, cost, and longer battery life. These requirements are, however, in conflict with the desired performance characteristics of higher data rate, increased capacity, multifunctionality and improved robustness.

Mm-wave frequency range provides an increase in capacity by offering a very broad bandwidth (BW) and high data rates. However, the associated propagation losses at mm-wave become too severe to ignore. Propagation loss is a strong function of frequency, i.e., as the frequency goes up so does the propagation loss. Moreover, the Oxygen Absorption Band (57-64 GHz) coincides with the unlicensed band of 59-64 GHz, which adds severe

absorption loss. Because of these problems, the development of antenna systems with high gain and beam-steering capability to achieve reliability is required. Phased array antennas with excellent beam-steering capability and high gain can provide the desired antenna properties [8–11]. This solution, however, comes with extremely high cost and increased system complexity, which may be prohibitive for practical and commercial wireless communication applications.

The multifunctional reconfigurable antenna (MRA) with beam-steering capability presented in this dissertation has the potential to be the main building block of a new class of mm-wave antenna array with low-cost and reduced complexity [12]. The main novelty of such a multifunctional reconfigurable antenna array (MRAA) lies in its variable element factor which is fixed for legacy phased array antennas. Recently, substrates such as SU-8 ($\varepsilon_r = 3.1$, $\tan\,\delta = 0.021$) which provides some advantages in terms of micro-fabrication have been used [13–15] in developing mm-wave antennas, however, SU-8 does not have optimal material properties (very high RF losses) for RF/antenna applications. On the other hand, SU-8 can be easily processed to form air cavities within, thereby taking advantage of the excellent material properties of air [16]. A micro-fabricated SU-8-based patch antenna structure exploiting air cavities was recently reported to achieve 57-66 GHz bandwidth and a maximum realized gain of 6.4 dBi [17].

This work targets accomplishing the design, manufacturing, and initial characterization of novel single element MRA and 2×8 planar MRAA prototypes. The design strategy aims to combine the advantages of multiple approaches of previous works [18, 19], as well as introducing a new approach. The design makes use of coplanar waveguide (CPW) loop feeding mechanism on quartz substrate to provide a broad BW. It uses low cost pyrex material where air cavities are easily formed by a single process step which does not only reduce cost but also take advantage of good RF properties of air. It is worth noting that this approach is simpler and less costly in terms of micro-fabrication as compared to forming air cavities in SU-8 which requires highly optimized multiple process steps. The MRA structure takes advantage of a low-cost and micro-fabrication process compatible pyrex

substrate material, which is used to fabricate reconfigurable parasitic layer. Considering a typical link-budget requirement at 60 GHz gigabit link [20], a maximum antenna gain of at least 15 dBi is needed. Therefore, it becomes proper to use array structure with at least 16 elements [21]. In this work, a 2×8 patch antenna array is presented. This array achieves 19.3 dBi maximum realized gain and $\sim 17\%$ impedance BW (57-65 GHz). The realized gain over the impedance bandwidth remains relatively flat changing from 17 - 19.3 dBi. This work targets establishing a 2×8 planar MRAA operating within the same band.

The parasitic layer based MRA presented in this dissertation consists of CPW-fed legacy patch antenna with a reconfigurable parasitic layer placed above it. The surface of parasitic layer has a grid of 3×3 electrically-small rectangular shaped metallic pixels. The adjacent connection/disconnection of the pixels gives the MRA variable element factor which results in reconfigurability in radiation properties. One of the challenges associated with using parasitic layer based MRA design is the interconnections of the metallic pixels. The operational characteristics of RF transistors and switches in lower frequencies ($\leq$ 15 GHz) are well-studied, but still under investigation for mm-wave spectrum. Another challenging issue associated with high frequency RF switches is the use and integration of components with exceedingly small dimensions. This makes the micro-fabrication and integration of the switches in mm-wave quite demanding. In [22], the authors have proposed Radio Frequency Microelectromechanical Systems (RF-MEMS) switches for mm-wave applications. However, stiction is a major concern for DC-contact switches with metal-to-metal contact [23], particularly in higher frequencies where the state changes occur more frequently. To this end, we investigate various switching technologies, such as RF transistors, p-i-n diodes, and smart material based switching designed to operate at 60 GHz.

The rest of the dissertation is organized in the following way: In Chapter 2, the dissertation objectives and research flow for each of the objectives have explained. From Chapter 3 to Chapter 7, the five dissertation objectives have been carried out with detailed simulations, design methodologies and characterizations. Finally, the dissertation is concluded in Chapter 8 with future research directions.

CHAPTER 2

DISSERTATION OBJECTIVES

The objectives of this dissertation are as follows:

1. Design, fabrication, and characterization of a standalone 60 GHz antenna.
2. Design, fabrication, and characterization of a parasitic layer based MRA with beam steering capability operating over $57 - 64$ GHz band.
3. Design, fabrication, and characterization of broadband high-gain 60 GHz 2×8 planar antenna array.
4. Design of 4×1 linear MRAA operating at 60 GHz Band.
5. Investigation and simulations of various switch technologies for MRA integration.

2.1 Research Flow for Objective 1

The first objective of this dissertation is to design, fabricate, and characterize single element antenna with a resonance frequency of 60 GHz. The motivation that leads to this objective is the necessity to build a legacy single element antenna that is simple enough to use as the reference device which will be modified to more sophisticated designs of MRAs, legacy arrays, and MRAAs. As the basic building block, this reference antenna will feature decent radiation properties. The designed broadband patch antenna is capable of covering the entire IEEE 802.11ad (WiGig) frequency band 57-66 GHz. Coplanar waveguides (CPWs) are capable of providing extremely high frequency response 100 GHz or more [24]; since the dispersion is very low and there is no need for via holes, which reduces undesirable parasitic inductance. Therefore, CPW is chosen as the appropriate feed mechanism in this design. The CPW-fed loop slot couples the energy efficiently to the patch antenna, resulting in a broad bandwidth. The patch metal is deposited on top of the pyrex substrate. The

main role of the pyrex material is to provide a reliable mechanical support for the patch metal, with an air cavity underneath, thus resulting in cumulative antenna substrate with very low loss, which leads to improved antenna performance. The simulated and measured impedance characteristics agree well, showing $\sim 15\%$ bandwidth. The simulated radiation pattern gains over the entire WiGig band 57-66 GHz demonstrate the integrity of radiation patterns with good gain values (average ~ 8.5 dB). Chapter 3 of this dissertation provides a detail discussion on the design method for this single element antenna.

2.2 Research Flow for Objective 2

In communication systems it is always desirable to have LOS propagation; at high frequencies this is ever more critical as the non-line of sight (NLOS) propagation losses are quite severe. Beam-steering is one of the most essential property desirable for LOS communication. After designing the single element legacy patch antenna, the next objective of this work is the design, micro-fabrication, and characterization of a multifunctional reconfigurable antenna with beam steering capability operating at 60 GHz band 59-66 GHz. The MRA provides three beam directions pertaining to: $\theta \in \{-30^0, 0^0, 30^0\}$; $\phi = 90^0$, based on reconfigurable parasitic layer approach. The structure consists of three layers, namely, feed, driven antenna, and reconfigurable parasitic layers. The feed mechanism is being kept the same as the single element antenna. The first two layers use RF and micro-fabrication process compatible quartz ($\varepsilon_r = 3.9$, $\tan\,\delta = 0.0002$) substrate while the parasitic layer is formed on a low-cost pyrex ($\varepsilon_r = 4.9$, $\tan\,\delta = 0.01$) material with air cavities formed underneath. The upper surface of pyrex has 3×3 rectangular shaped metallic pixels; four of them are interconnected by RF switch component. This choice minimizes the number of switch interconnections on the reconfigurable pixel parasitic while enhancing the beam diversity. By judiciously controlling the switch status the beam-steering is accomplished. The simulated impedance and gain characteristics show $\sim 15\%$ bandwidth over which the maximum realized gain remains relatively flat around ~ 7.2 dB for all modes of operation. Further detailed discussion of this design is provided in Chapter 4 of this dissertation.

2.3 Research Flow for Objective 3

Before designing the MRAA, the next objective is to design a legacy patch antenna array which will act as a reference design for the MRAA prototype. Compared to single element patch antenna, an antenna array inherently provides higher broadside gain. In Chapter 5, the design techniques, fabrication procedures, and characterization of a 2 × 8 patch antenna array operating in the IEEE 802.11ad frequency band (57-66 GHz) is presented. The design is based on two-layer structures, where the radiating patches placed on top substrate are fed by conductor backed coplanar waveguide (CPW)-fed loop slots, which are placed on the bottom substrate. The top layer is formed by using a low-cost pyrex ($\varepsilon_r = 4.9$, $\tan\,\delta = 0.01$) substrate of 500 μm thickness. The pyrex is then etched down to a thickness of 100 μm using HF-based chemical wet-etch process where 400 μm of air volume is formed underneath. This approach does not only benefit from the low-cost feature of pyrex but also exploits the low-loss nature of air. The thin layer of pyrex is solely used for mechanical support for the radiating patches while the air provides good RF environment for the array. The bottom substrate housing the CPW feed network is an RF-compatible quartz ($\varepsilon_r = 3.9$, $\tan\,\delta = 0.0002$) of 525 μm thickness. The simulations indicate a good gain performance of 19.3 dBi maximum realized gain. The variation of the realized gain over $\sim$ 17% of impedance bandwidth 57-65 GHz is relatively constant changing from 17-19.3 dBi.

2.4 Research Flow for Objective 4

The fourth objective is to design, fabricate, and characterize an MRAA with a resonance frequency of 60 GHz. MRA presented in Chapter 4 acts as a building block for this MRAA and is designed by creating a linear array of four identical MRAs. The distances between the antenna elements are optimized to increase the broadside gain. The designed corporate feed network ensures that the elements are fed with equal phase. The feed network and driven patch antennas are placed on two separate layer of quartz ($\varepsilon_r = 3.9$, $\tan\,\delta = 0.0002$) substrate with thickness of 525 μm and 260 μm respectively. On top of this driven antenna structure the parasitic layer was formed with rectangular grid of metallic

pixels that lay on a 500 μm thick pyrex ($\varepsilon_r = 4.9$, tan $\delta = 0.01$) substrate. Height of the parasitic layer and inter pixel distance is optimized to maximize the antenna performance. The MRAA has three different beam directions (modes of operation) pertaining to: $\theta \in \{-30^0, 0^0, 30^0\}$; $\phi = 90^0$. The simulated impedance and gain characteristics show wide bandwidth over which the maximum realized gain remains relatively flat around $\sim$ 13.5 dB for all modes of operation. To increase the beam-steering capability, another MRAA is designed which is capable of operating in three different beam directions pertaining to: $\theta \in \{-50^0, 0^0, 50^0\}$; $\phi = 90^0$. This design has been optimized to improve beam steering performance using a simpler pixel layer geometry and as a result has less pixels and pixel interconnections when compared to the original design. The trade-off comes from the realized gain; the simulated gain characteristics show that the maximum realized gain is around $\sim$ 12 dB. The detailed design procedure of these two MRAAs structure are presented in Chapter 6.

2.5 Research Flow for Objective 5

One of the aspects that needs to be considered while designing MRAs/MRAAs is the RF-switching technology. There are many competing switch technologies that can be used for the MRAs/MRAAs designed thus far. Among others, micro-fabrication compatibility, cost, RF performance and monolithic integration are the main factors to consider in adapting the most suitable technology. To this end, we will investigate rather mature switching technologies like p-i-n diodes, RF transistors, as well as new emerging material technologies, e.g., smart material based switching via metal-insulator transition compounds such as vanadium oxide (VO_2). VO_2 is a phase change (chalcogenide) material, which changes its resistivity when exposed to heat, thus, essentially working as switch with low ON state resistance (at high temperature) and high OFF state resistance (at low temperature). In Chapter 7 of this dissertation, all these switching technologies are presented. Through simulations and measurements, pros and cons of each switching technology is determined. Simulation results for smart material, i.e., VO_2 and p-i-n diodes are presented.

CHAPTER 3
SINGLE PATCH ANTENNA ELEMENT BASED ON QUARTZ AND PYREX MATERIALS

3.1 Introduction

The fundamental problem in wireless network is to provide ever-increasing total wireless throughput reliably and uniformly throughout a designated area. In the near future, because of the explosion in data traffic, demands that need to be addressed are increased capacity, improved data rate, decreased latency, and better quality of service. To meet these demands, drastic improvements need to be made in the existing wireless network architecture. As the current physical layer technologies are already operating at the boundary of Shannon capacity, the solutions seem to be the exploitation of mm-wave spectrum and increase of access points covering smaller area, i.e., small cells. Exploitation of mm-wave spectrum not only increases the available bandwidth but also provides an excellent choice for smaller cells [25]. As the front end of any wireless communication systems, mm-wave antenna design, optimized over directional gains, cost, and complexity is crucial and has attracted a lot of attention from the research community [26].

Antennas operating at mm-wave frequencies have thus far mainly been fabricated using low temperature co-fired ceramic (LTCC) [27–29], polymer substrates [30] and SU-8 material [17]. Although LTCC can create mechanically robust and hermetically sealed packages with high yield, it might create unwanted surface waves due to the high dielectric constant of substrate [31]. Recently, planar antennas have also been realized on benzocyclobutene (BCB) polymers at mm-waves [30]. BCB ($\varepsilon = 2.65$, $\tan \delta = 0.0008$), due to its electrical properties, is a good alternative substrate material for improved antenna performances. However, it is quite difficult to achieve the desired thickness with BCB that is needed for obtaining a reasonable operational bandwidth at high frequencies. Moreover, very short

shelf-life time under room temperature is another disadvantage [31]. Taking all these factors into account, quartz appears as a highly RF-compatible material which is commercially available in standard wafer sizes. Quartz is a micro-fabrication compatible substrate that has a suitable dielectric constant and very low loss tangent ($\varepsilon_r = 3.9$, $\tan\,\delta = 0.0002$ at 60 GHz). This chapter of the dissertation presents a patch antenna that is micro-fabricated on such quartz substrates. The antenna presented here is designed to have a broadband radiation and aims to cover the entire IEEE 802.11ad (WiGig) frequency band (57-66 GHz).

3.2 Antenna Design

The antenna (as shown in Fig. 3.1 and 3.2), is a coplanar wave guide (CPW) fed broadband patch antenna micro-fabricated on an RF compatible quartz substrate. The feed metallization, which consists of a 50 Ω conductor backed CPW, along with the loop, is formed on a 525 μm thick quartz substrate. The CPW structure in Fig. 3.3 consists of a center strip with two parallel ground planes placed equidistant from it on either side. All three conductors in the CPW are located on the same side of the substrate surface. The dimensions of the center strip, the gap, the thickness, and permittivity of the dielectric substrate determined the effective dielectric constant, characteristic impedance and the attenuation of the line. The gap in the CPW is usually very small and supports electric fields primarily concentrated in the dielectric. With little fringing field in the air space, the CPW exhibits low dispersion [32].

The pyrex substrate ($\varepsilon_r = 4.9$, $\tan\,\delta = 0.01$ at 60 GHz) is located on top of the quartz layer. The patch antenna metallization is finally formed on this substrate. Pyrex material which is thinned down to 100 μm by using standard chemical wet-etch process is incorporated to decrease the dielectric loss which would in turn enhance the performance of the antenna. The height of the air pocket(A_t) formed under the thinned pyrex, has an effect on the impedance BW and realized gain of the antenna [19, 33–35]. To enhance the BW of patch antenna a conductor backed CPW-fed rectangular loop slot (with dimensions L_l, L_w, and L_t) shown in Fig. 3.4 couples the energy to the patch antenna. The resonant length of the loop is calculated as:

$$L_1 + \frac{L_w}{2} \approx \frac{\lambda_g}{2} \tag{3.1}$$

where λ_g is the guide wavelength in quartz substrate at the resonant frequency (f_s). The substrate thickness of conductor backed CPW fed loop slot plays an important role in broadening the radiation BW of the antenna. One of the main contributions of this dissertation is not only to improve the antenna performance in the WiGig band but also to make the antenna design compatible with micro-fabrication processes, resulting in efficient, reliable and mass-production compatible economic fabrication. The patch antenna dimensions are then calculated accordingly by using the following [36]:

$$P_l \approx \frac{c}{2f_p\sqrt{\epsilon_r}} \tag{3.2}$$

$$P_l < P_w < 2P_l \tag{3.3}$$

where P_l and P_w represent the patch length and width (see Fig. 3.1), c is the speed of light in vacuum, and f_p is the patch design frequency, and ϵ_r is the relative permittivity of the material. The optimized design parameters of the patch element, CPW-fed loop, and the pyrex substrate were obtained from full-wave simulations are provided in Table 3.1. This design methodology minimizes the dielectric loss of pyrex through air pockets resulted in better performances. Secondly, the patch metallization on top of the pyrex substrate focuses the EM energy resulting in a narrower beamwidth, which is otherwise broader for a standard CPW-fed loop.

3.3 Simulation Results and Characterizations

The simulated magnitudes of the reflection coefficient (S11 parameter) for a frequency range from 55 to 67 GHz is plotted in Fig. 3.5. The reflection coefficient shows that the antenna has a 2:1 VSWR BW of greater than 9 GHz ($\sim$ 15% of fractional BW), which covers the entire frequency range of the IEEE 802.11ad (57 - 66 GHz). The simulated

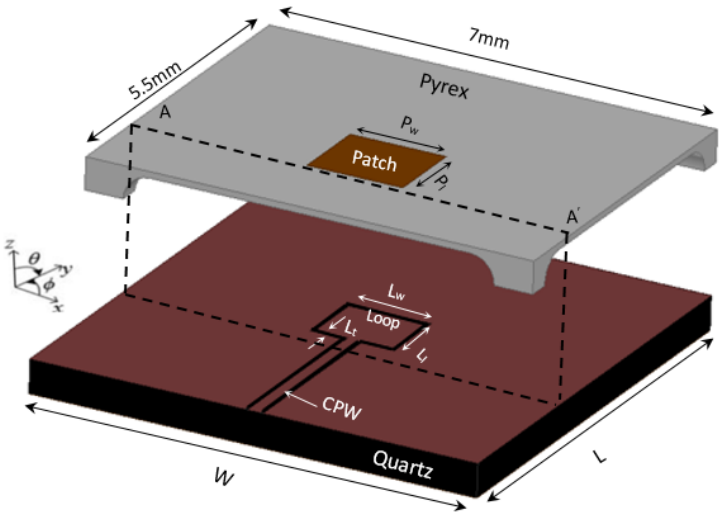

Fig. 3.1: Schematic depicting 3-D drawing of the antenna (For the sake of illustration, the pyrex layers is suspended on top of the CPW metallization).

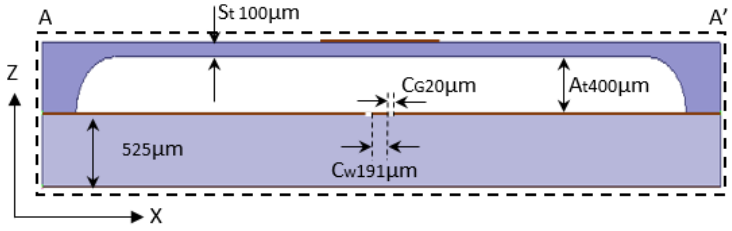

Fig. 3.2: Schematic showing cross-sectional drawing of the single-element two-layers antenna.

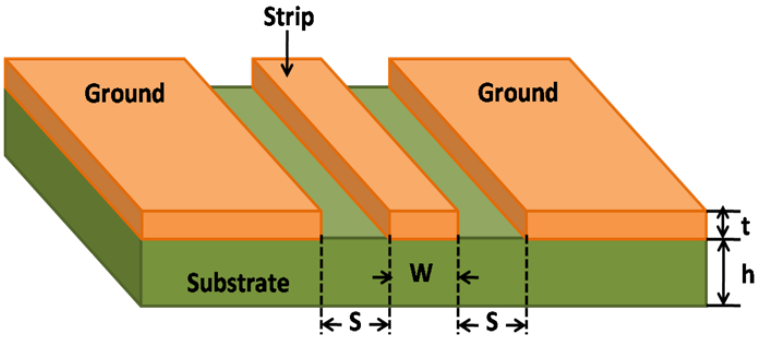

Fig. 3.3: Coplanar wave guide design. The width of the central conductor (W), the gap from the ground planes (S), the substrate thickness (h), the conductor thickness (t).

Table 3.1: The critical design parameters of the WiGig antenna (all dimensions are in mm).

W	7	P_w	1.5	L_l	1	C_G	0.02
L	7	P_l	1.3	L_w	1.2	C_w	0.191
L_t	0.02	S_t	0.1	A_t	0.4		

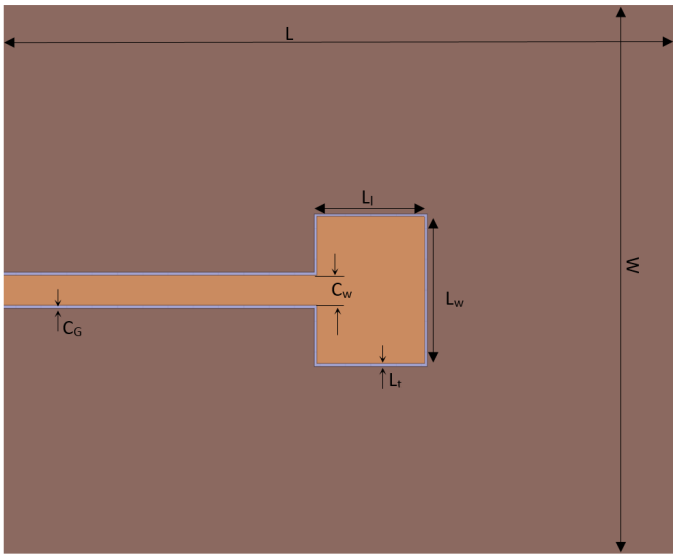

Fig. 3.4: Top view of CPW layer (Loop is centralized w.r.t. CPW layer).

radiation patterns of the linearly polarized antenna in y-z plane at 60 GHz are shown in Fig 3.6. The realized maximum gain of the antenna stays relatively constant and is in the range of $8.4 - 8.7$ dB over the entire BW as shown in Fig. 3.7. The antenna design has been recently fabricated. Second phase of the design for fine tuning the antenna performance will be determined after the measurement results are available.

3.4 Micro-Fabrication

3.4.1 Quartz Substrates

Prior to fabrication, RF-compatible and low-loss quartz substrates ($\varepsilon_r = 3.9$, tan $\delta = 0.0002$ at 60 GHz) were cleaned using standard acid/solvent cleaning, distilled water (DI)-water rinsing, nitrogen-blow drying, and de-hydration baking on a 120^0 C hot-plate. The quartz wafer was primed by spraying with MCC primer (20% hexamethyldisilazane

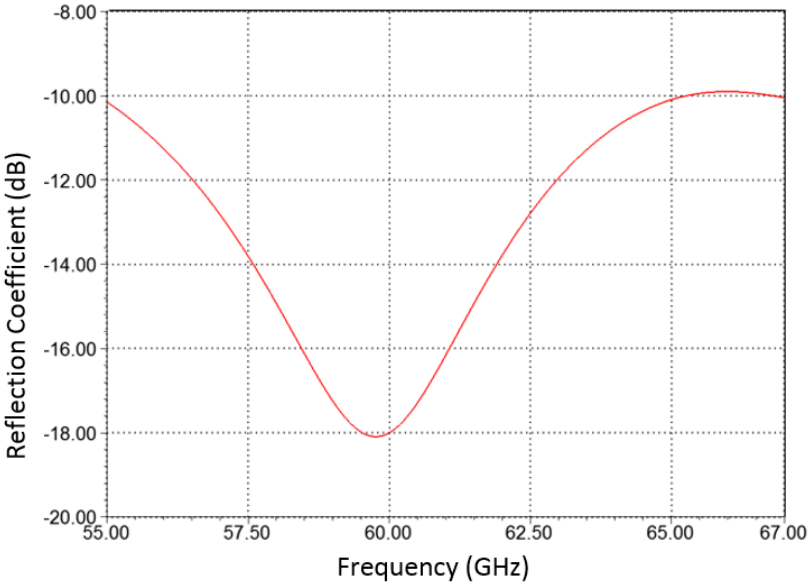

Fig. 3.5: Simulated reflection coefficient (S11 parameter) of the single element antenna for frequency range of 55 to 67 GHz.

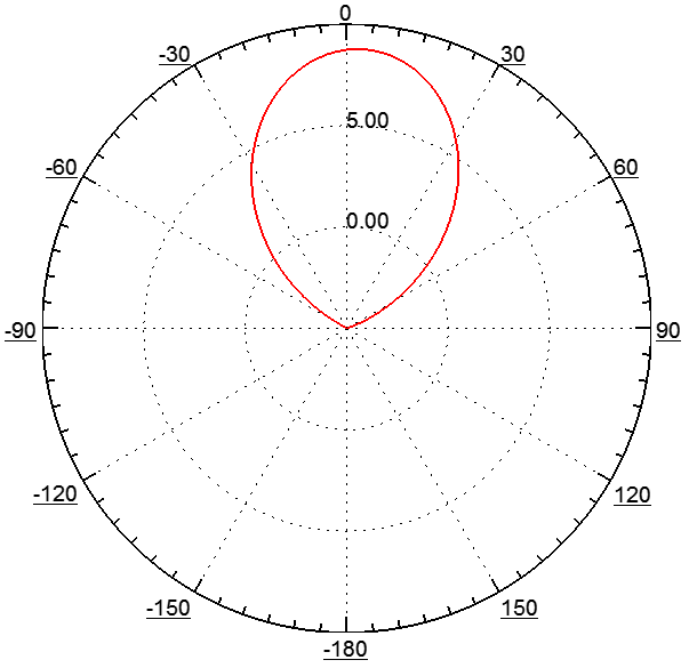

Fig. 3.6: Simulated realized gain plot (dB) of the single element antenna in y-z plane at 60 GHz.

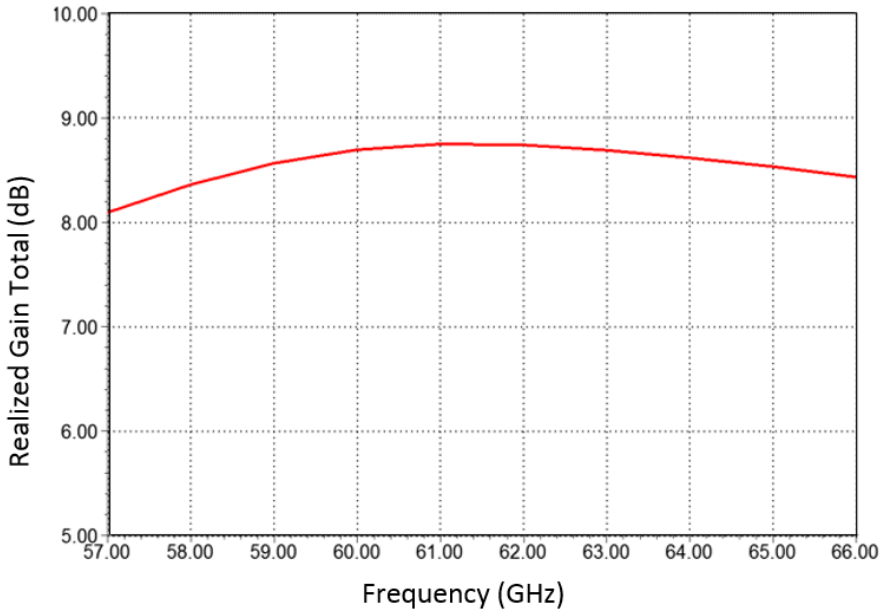

Fig. 3.7: Simulated realized gain (dB) in the broadside direction of the single element antenna with respect to frequency.

(HMDS)) and (80% propylene glycol monomethyl ether (PM) acetate on a spin coater which was run at 2000 revolution per minute (rpm) for 20 seconds. Then the wafer was baked at 110^0 C for 90 seconds. After spin coating, the wafer was sprayed with photo-resist (PR) ($AZ4562$) and spin dried for 45 seconds at 3000 rpm. Afterwards, the wafer was pre-baked for 20 minutes at room temperature and baked for 50 seconds at 110^0 C. The wafer was exposed to ultraviolet(UV) light to pattern CPW, loop, and bonding alignment marks. After exposure, the wafer was developed by introducing the wafer into $AZ400K$ solution. Oxygen (O_2) plasma was then applied for 15 seconds to remove possible photo-resist residue and to clean the wafer surface. The wafer was coated with Chromium (25 nm)/Copper (1 μm)/Gold (50 nm) (Cr/Cu/Au) and then lift-off was done by dipping the coated wafer into acetone. In addition, blank Copper deposition was carried out to form the ground layer at the backside of the wafer. The micro-fabricated CPW and ground on this quartz is shown in Fig. 3.8. Finally, quartz wafer was diced to achieve the final sample structure.

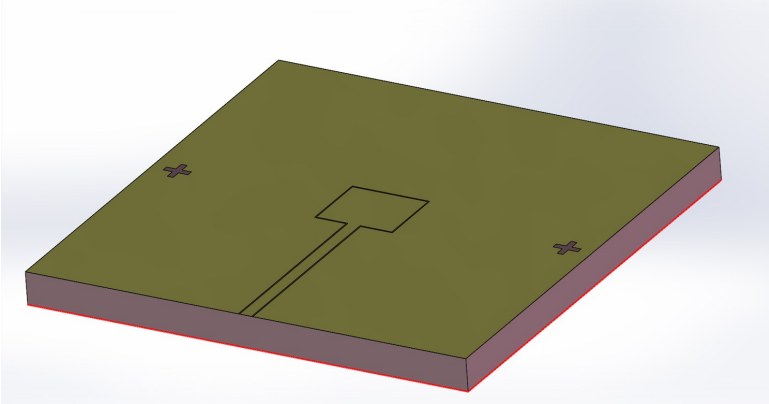

Fig. 3.8: Micro-fabricated CPW and ground layer with standard deposition and liftoff process.

3.4.2 Pyrex Substrates

The pyrex wafer was spin-coated with PR ($AZ4562$) and spin dried for 45 seconds at 3000 rpm. Then the wafer was prebaked for 20 minute at room temperature and baked for 50 seconds at 110^0 C. After coating the wafer with PR, it was exposed to UV light to pattern patch and bonding alignment marks as shown in Fig. 3.9. After exposure, the wafer was developed in $AZ400K$ developer solution. To remove possible PR residue and clean the sample surface, O_2 plasma was applied for 15 seconds. The wafer was coated with 30/400/100 nanometer (nm) thick Cr/Cu/Au by using e-beam evaporator and then metal lift off was done by dipping the wafer into acetone. To obtain a uniform surface, deposition rate and rotation of the sample are important parameters. We used $\sim 0.3 - 0.4$ nm/sec deposition rate for each metal. The backside of the wafer is coated with PR ($AZ4562$) and baked for 90 seconds at 110^0 C. After coating the wafer with PR, it was exposed to UV light to pattern patch and bonding alignment marks. After exposure, the wafer was developed similarly in $AZ400K$ solution.

The micro-fabricated patch antenna metallization on this pyrex is shown in Fig. 3.10. Finally, pyrex wafer was diced to achieve the final sample structure of the single-element two-layers antenna. The backside of the wafer was then etched with a special grinder-blade by using dicing-saw to create the air space. The fabricated antenna prototype is shown in Fig 3.11.

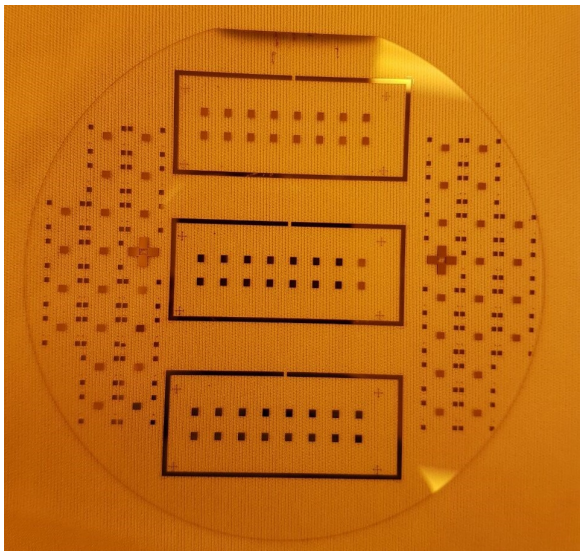

Fig. 3.9: Patterned wafer with patch and alignment marks.

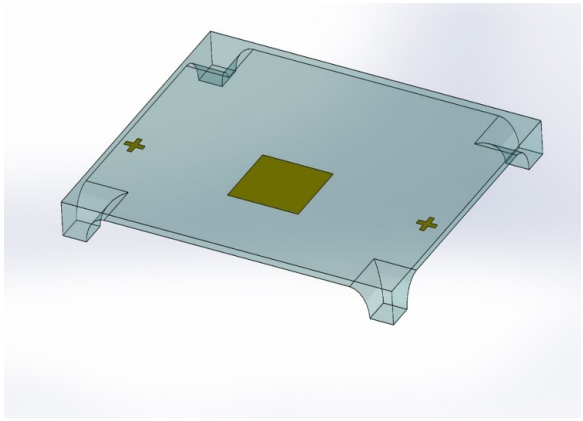

Fig. 3.10: Micro-fabricated patch antenna metallization on the pyrex.

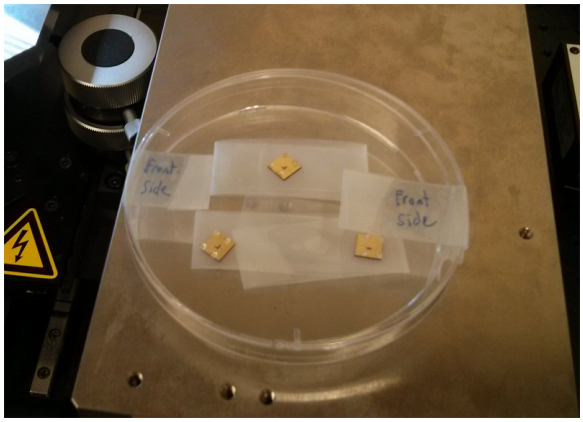

Fig. 3.11: Prototype of single element 60 GHz antenna.

3.5 Conclusion

The design, micro-fabrication, and characterization of a CPW-fed broadband patch antenna compatible with IEEE 802.11ad standard (WiGig) has been successfully demonstrated. The simulated impedance characteristics show $\sim 15\%$ bandwidth. Also, the simulated radiation pattern results demonstrate the integrity of radiation pattern with decent gain values (~ 8.5 dB) in the broadside direction over the entire WiGig band ($57-66$ GHz). This result confirms the success of our design in using low dielectric-loss medium. The pyrex micro-fabrication processes developed for this antenna structure provides an important advantage for custom-made reconfigurable antennas that might also be highly useful in WiGig applications.

CHAPTER 4
DESIGN, FABRICATION, AND CHARACTERIZATION OF A PARASITIC LAYER BASED MRA WITH BEAM STEERING CAPABILITY OPERATING OVER 57-64 GHZ BAND

4.1 Introduction

Due to the scarcity of spectrum at the lower end and the possibility of high data rate communication, 60 GHz band has attracted a lot of interest in recent years. While this mm-wave frequency range is excellent in offering very broad bandwidth (BW) and high data rates, the associated propagation losses are too severe to ignore. Wireless networking among multiple devices at gigabits per second (Gb/s) data rates which is an order of magnitude faster than Wi-Fi is the goal that standardization activities have set for 60 GHz technology [37]. One of the intriguing challenge for an antenna engineer is to design high performance antennas suitable for such high frequencies. The 60 GHz carrier frequency results in substantial propagation loss at a given range (e.g., 82 dB at 5 m [38]), combined with increased shadowing, makes NLOS communication very challenging. A desired communication path must be found to avoid signal blockage by common objects for LOS communication. This makes the development of antenna systems with high gain and beam-steering capability a necessary engineering task.

Phased array antennas with excellent beam-steering capability and high gain can provide a desired antenna properties [8,39–41]. Since the phase shift usually is obtained through the introduction of additional path length, one of the problems that arises with a phased array is insufficient bandwidth. Particularly, at this range where the desirable bandwidth can be as high as 7 GHz (57-64 GHz), this can cause a severe problem [42]. High cost and complex array architecture, excess RF losses in the corporate feed networks, problems associated with high density device integration and need for heat removal makes the choice

of active phase array antennas unattractive for multi-beam communications. The MRA with beam-steering capability presented in this dissertation has the potential to function as the main building block of a new class of mm-wave antenna array with low-cost, low-size and reduced complexity [12]. The main novelty of such a reconfigurable antenna array is its variable element factor which is fixed for legacy phased array antennas. This work presents the design, manufacturing, and initial characterization of a single element MRA. This MRA structure takes advantage of low-cost and micro-fabrication process compatible pyrex substrate, which is used to create innovative reconfigurable parasitic layer.

4.2 MRA Structure and Working Mechanism

The MRA structure as shown in Fig. 4.1 and Fig. 4.2, is designed to reconfigure the main beam direction of the radiation pattern into three different directions pertaining to: $\theta \in \{-30^0, 0^0, 30^0\}$; $\phi = 90^0$ over $59 - 66$ GHz band. The antenna structure consists of three layers namely, the feed, the driven antenna, and the reconfigurable parasitic layer with respective thicknesses of 525 μm, 260 μm, and 500 μm. The bottom and middle layers which house the CPW-fed loop and driven patch antenna, respectively, are formed on quartz substrates which provide good RF properties and micro-fabrication process compatibility. The CPW-fed loop couples the EM energy to the patch antenna, which results in a broad BW. The formation of copper metalization for both layers are implemented by basic micro-fabrication processes of thin layer metal deposition via electron-beam evaporation and lift-off techniques. The top layer is made out of low cost pyrex material which is thinned down to 100 μm by using standard chemical wet-etch process. The upper surface of this layer has 3×3 metallic rectangular shaped pixels, which are connected or disconnected by means of switching. As the initial step and for the sake of simplicity, these interconnections are employed as perfect short and open circuits (i.e., ideal ON/OFF switch conditions) in this work. Among the total of twelve interconnections between adjacent pixels only four needed to be controlled to accomplish the targeted three different beam-steering directions [27, 43].

This layer is solely used for mechanical support for reconfigurable pixel surface and the air cavity formed underneath with a thickness of 400 μm serves as low dielectric constant

and low loss medium. The design parameters are jointly optimized to simultaneously yield broad impedance BW, high gain and desired beam steering capability. The optimized design parameters of the patch element, CPW-fed loop, and the reconfigurable parasitic layer which are obtained by full-wave EM simulations are provided in Table 4.1.

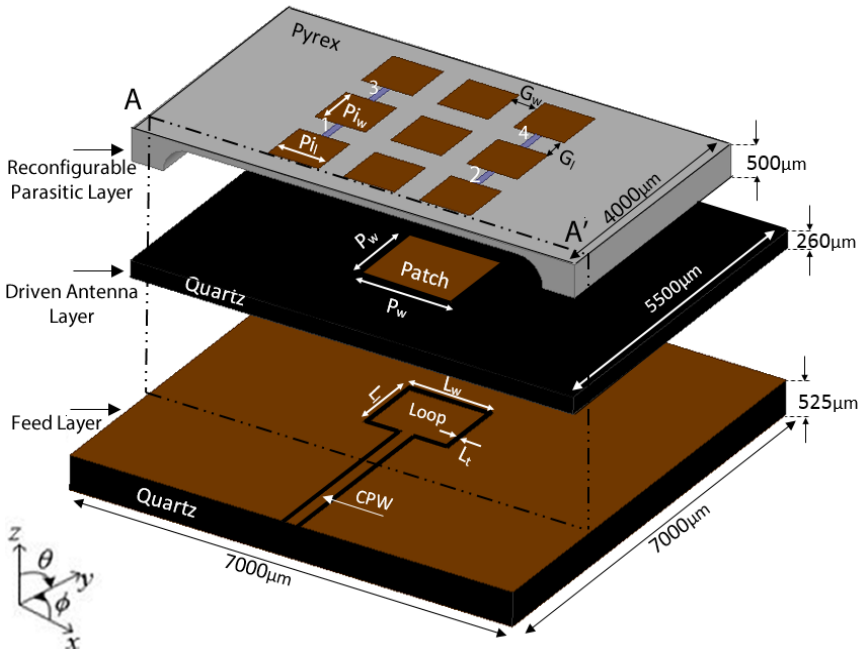

Fig. 4.1: 3-D Schematic of the designed MRA (for illustration purpose the layers are suspended on top of each other), 1, 2, 3, 4 denote switch's location.

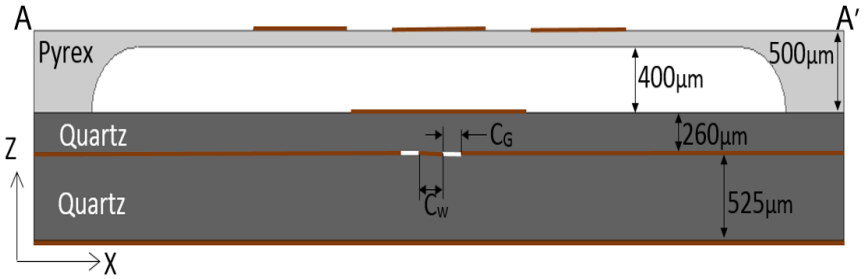

Fig. 4.2: A-A′ cross section view of the radiation pattern reconfigurable antenna.

Table 4.1: The critical design parameters of the mm-wave MRA (all dimensions are in mm).

Pi_l	0.8	Pi_w	0.8	G_l	0.4	G_w	0.4
P_w	1	L_l	0.7	C_G	0.02	C_w	0.191
P_l	1	L_w	0.8	L_t	0.02	S_t	0.1

4.3 Simulation Results and Characterization

The top view of the MRA showing switch locations is depicted in Fig. 4.1. A multi-objective genetic algorithm optimization [44] in conjunction with full-wave analysis is used to design the reconfigurable parasitic surface. Results indicate that only four out of twelve interconnections need to be controlled in order to achieve the targeted three beam steering directions pertaining to: $\theta \in \{-30^0, 0^0, 30^0\}$; $\phi = 90^0$over $59 - 66$ GHz band. The corresponding optimized switch configurations are given in Table 4.2.

The simulated reflection coefficients for all the three modes of operation are given in Fig. 4.3. The intersection of three individual reflection coefficients indicate a common BW of $\sim$ 6 GHz covering $59 - 65$ GHz band. The total realized gain patterns in y-z plane corresponding to each mode of operation at 60 GHz are shown in Fig. 4.4. The maximum realized gain values in the steered beam directions are all above $\sim$ 7 dBi. The realized gain values for all modes of operation over the entire $59 - 64$ GHz band are in the range $\sim 6.5 - 7.9$ dB as shown in Fig. 4.5.

The fabrication of this MRA is already under progress and measurement of the fabricated antenna will be performed as soon as the fabrication is completed. Based on the measured performances, there might be a second run for the design aspect as some of the design parameters may need fine tuning.

4.4 Micro-Fabrication

4.4.1 Quartz Substrates

The fabrication technique used for quartz remains same as mentioned in Section 3.4.1. However, it is worth mentioning that, MRA design presented in this chapter has two quartz layers, namely feed layer and driven antenna layer (Fig. 4.1). As mentioned earlier, the 260

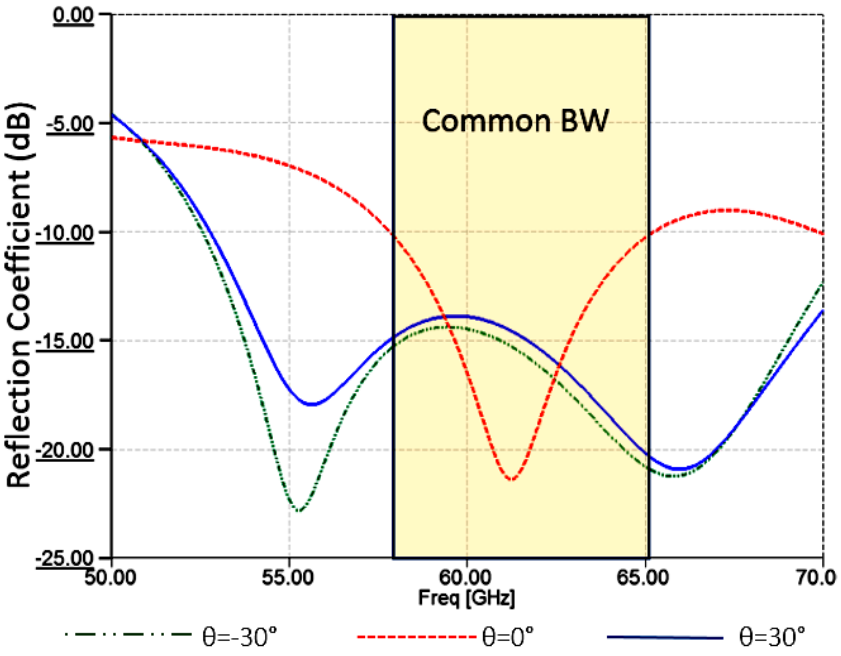

Fig. 4.3: Simulated reflection coefficient of the MRA.

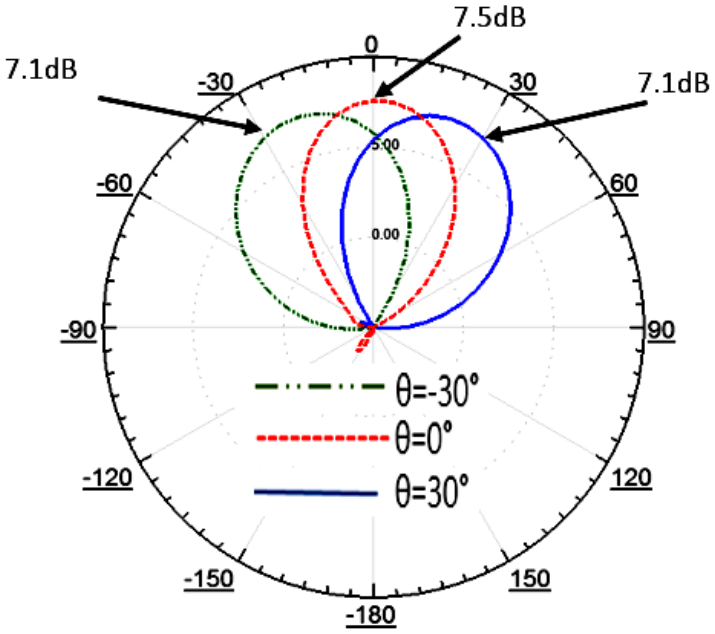

Fig. 4.4: Simulated total realized gain plots of the MRA in $\phi = 90^0$ $(y-z)$ plane.

Table 4.2: The switch status corresponding to three beam steering directions (0=OFF, 1=ON).

Switch Number	1	2	3	4
$\phi = 90^0, \theta = 0^0$	0	0	0	0
$\phi = 90^0, \theta = -30^0$	1	1	0	0
$\phi = 90^0, \theta = 30^0$	0	0	1	1

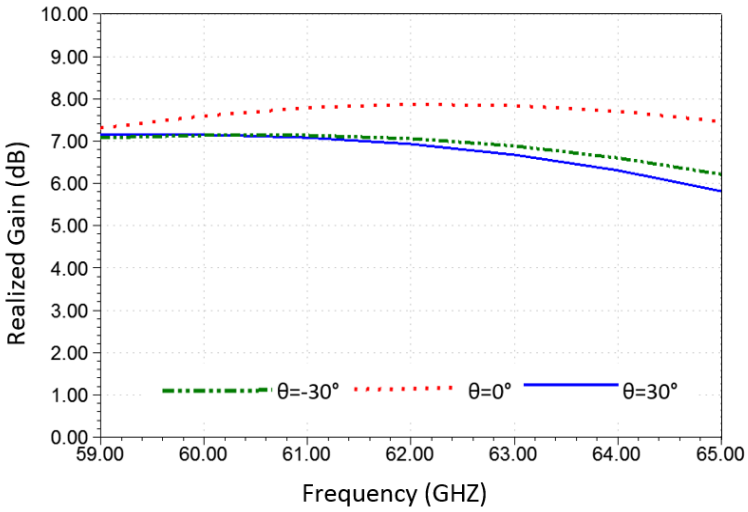

Fig. 4.5: Simulated realized gain values over 59-64 GHz band for three beam-steering directions $\theta \in \{-30^0, 0^0, 30^0\}$; $\phi = 90^0$ $(Y - Z)$ plane.

μm thick driven antenna layer sits on top of the feed layer which is 525 μm thick feed layer.

4.4.2 Pyrex Substrates

To create the reconfigurable parasitic later on a 500 μm thick pyrex substrate from which 400 μm was etched away, the fabrication technique mentioned in Section 3.4.2 in this dissertation was used.

4.5 Conclusion

A CPW-fed broadband MRA IEEE 802.11ad standard (WiGig) is designed, micro-fabricated, and characterized. The simulated radiation patterns shows reasonably constant gain of ~ 7 dBi in all modes of operations over the entire bandwidth. This micro-fabrication friendly and low cost MRA can be useful for small cell mm-wave applications.

CHAPTER 5
DESIGN, FABRICATION AND CHARACTERIZATION OF BROADBAND HIGH-GAIN 60 GHZ 2×8 PLANAR ANTENNA ARRAY

5.1 Introduction

Availability of unlicensed frequency band and possibility of high speed communication in short range have been attracting great interest for wireless communication systems operating at around 60 GHz commonly known as mm-wave or WiGig band [5]. However, the propagation losses associated with this band are severe, thus limiting the wireless communication coverage to short distances. Therefore, antennas with high gain are needed. The losses associated with conductors, dielectrics, and surface waves make designing an antenna with a high gain over a broad bandwidth quite challenging. Recently, substrates such as SU-8 ($\varepsilon_r = 3.1$, $\tan \delta = 0.021$) which provides some advantages in terms of micro-fabrication have been used. Although, SU-8 does not have good material properties (very high RF losses) for RF/antenna applications, it can be processed to form air cavities within, thereby taking advantage of good material properties of air [16]. A micro-fabricated SU-8-based patch antenna structure exploiting air cavities was recently reported to achieve $57 - 66$ GHz bandwidth and a maximum realized gain of 7 dBi [17].

Patch antennas inherently have small operational bandwidth (BW) [45], which can be improved by using different techniques such as employing a thick substrate with a low dielectric constant [46] or using stacked patch structure [47]. Also, a CPW-fed slot coupled patch approach can be used to enhance the BW of patch antennas [48]. Low temperature co-fired ceramic (LTCC) [49] has been utilized for implementing antennas operating at mm-wave frequencies. In [33], a 4×4 planar array operating at 60 GHz band, comprised of aperture coupled patch antennas built on multi-layer LTCC substrate was implemented. This array achieved 9.5% impedance BW and 18.2 dBi maximum gain. Despite mechan-

ical robustness and ease of packaging, LTCC creates unwanted surface waves due to high dielectric constant.

This work attempts to develop a low cost and high performance (broad impedance BW with high realized gain) antenna array working at 60 GHz. To this end, two-layer antenna structure using the combination of RF compatible quartz substrate and low-cost pyrex substrate is adopted. The design strategy is to combine the advantages of multiple approaches of previous works [18,19]. The design makes use of CPW loop feeding mechanism on quartz substrate to provide broad BW. It uses low cost pyrex material where air cavities are easily formed by a single process step which does not only reduce cost but also take advantage of very good RF properties of the air. It is worth noting that this approach is much simpler and cheaper in terms of micro-fabrication as compared to forming air cavities in SU-8 which requires highly optimized multi-step processes. Considering the link-budget requirement at 60 GHz gigabit link [20], a maximum antenna gain of at least 15 dBi is needed. Therefore, it becomes proper to use at least 16 element array designs. In this work, a 2×8 patch antenna array is presented. The inter-element distance of the array is optimized providing low mutual coupling and air bridges used in the feed network helps reduce RF losses by enabling continuous electric field across the T-junctions used. This array achieves a 19.3 dBi maximum realized gain and $\sim 17\%$ impedance BW ($57-65$ GHz). The realized gain over the impedance bandwidth remains relatively flat from $17-9.3$ dBi.

5.2 Antenna Array Design

The antenna structure as shown in Fig. 5.1 consists of two layers. The bottom layer uses quartz substrate which has good RF properties and is compatible with micro-fabrication processes. The feed metallization consisting of 50 Ω conductor backed (CB) CPW and the CPW-loop is formed on this layer. A pyrex substrate with a thickness of 500 μm was chemically etched to a thickness of 100 μm, which is used as support layer for the radiating patch elements. This thin pyrex layer is placed on top of the bottom layer. The volume of the air layer with a thickness of 400 μm under pyrex provides overall low dielectric constant along with low loss, which improves the impedance bandwidth and gain. The role of thin

pyrex layer is to provide mechanical support for radiating patches. The CB CPW-fed loop, patch size and element spacing are jointly optimized to get a broader BW and maximum realized gain, where the numerical values are given in Table 5.1. Corporate feeding network with power dividers has been utilized to excite each array element with equal power and phase. Necessary characteristic impedance transformations using quarter wave transformer have also been performed in the T-junction dividers.

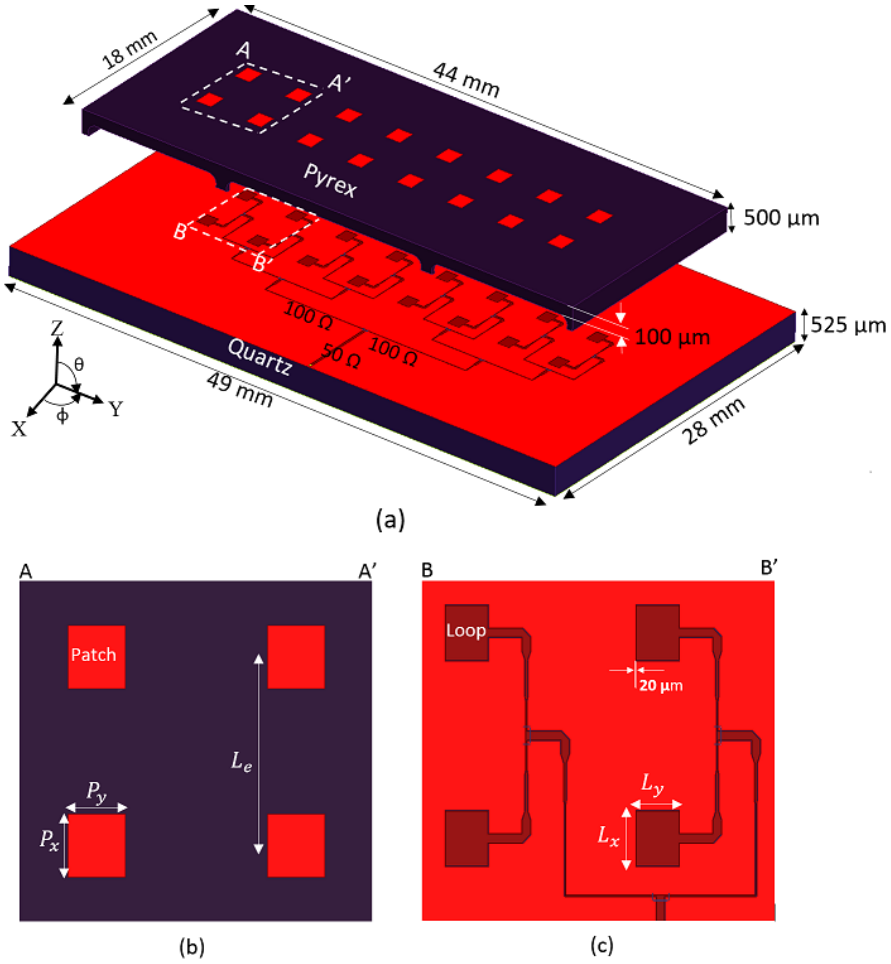

Fig. 5.1: (a) Schematic of 3-D structure of the antenna array, (b) Enlarged A-A′, (c) Enlarged B-B′.

Table 5.1: Design parameters (dimensions are in mm).

P_x	1.5	L_x	1.24	L_e	$0.7\lambda_0$
P_y	1.3	L_y	1.04		

5.3 Simulation Results and Characterization

Fig. 5.2 shows simulated reflection coefficient of the antenna, where a bandwidth of 10 GHz from $55-65$ GHz covering the frequency range of the IEEE 802.11ad is obtained. The simulated radiation pattern of the array in y-z plane at 59 GHz is shown in Fig. 5.3 The realized maximum gain of the array is relatively constant over the entire bandwidth which is in the range of $17-19.3$ dB, which is shown in Fig. 5.4.

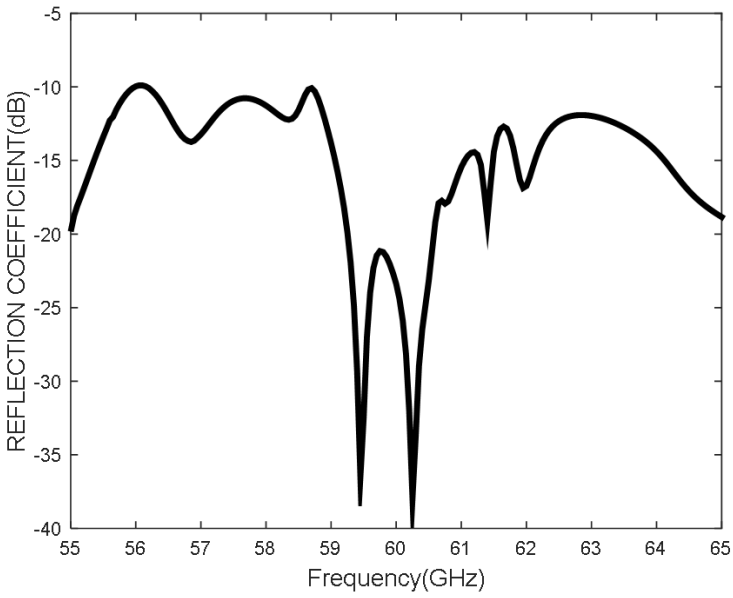

Fig. 5.2: Simulated reflection coefficient of the antenna array.

The micro-fabrication of this array is already under progress and measurement of the fabricated antenna will be performed as soon as the fabrication is completed. Fig. 5.5 shows the photo-mask layers designed for micro-fabrication of the antenna array. Based on the measured performances, there might be a need for a second run for the design aspect as some of design parameters may need fine tuning.

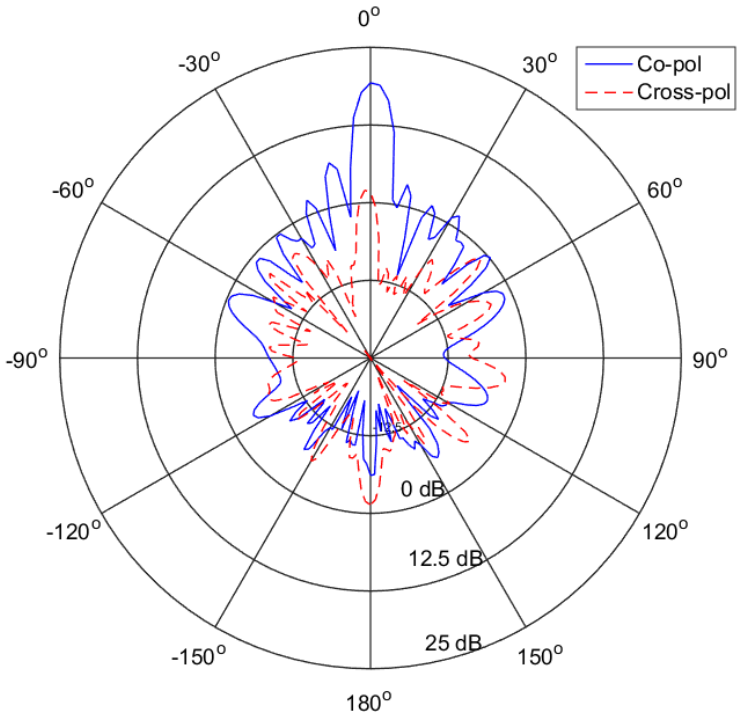

Fig. 5.3: Simulated radiation pattern of the linearly polarized antenna in $x-y$ and $y-z$ plane at 59 GHz.

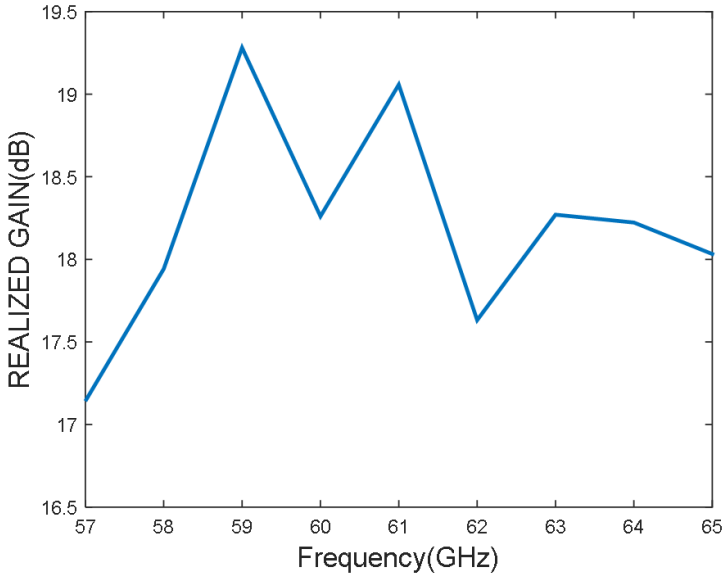

Fig. 5.4: Simulated realized gain values of the 2×8 Planar Antenna Array over $57-65$ GHz band.

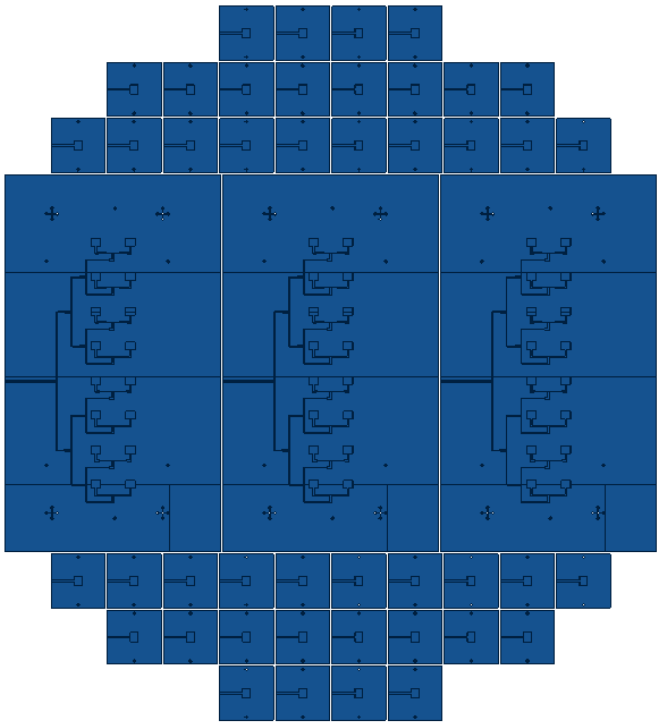

Fig. 5.5: Photo-mask designs for the micro-fabrication of the antenna array.

5.4 Conclusion

A CPW-fed patch antenna array compatible with IEEE 802.11ad standard has been designed. The simulation results indicate relatively constant gain values ($17 - 19.3$ dB) over $57 - 65$ GHz band, which makes the designed array a strong candidate for multi-gigabit applications. The micro-fabrication and characterization of the antenna is ongoing.

CHAPTER 6

DESIGN OF 4×1 LINEAR MRAA OPERATING AT 60 GHZ BAND

6.1 Introduction

An antenna array with beam steering capability is very advantageous to avoid noisy environments, maneuver away from electronic jamming, improve system gain, security and saving energy by directing signals only towards the intended directions. While phased array [50–52] can perform these tasks, its increased size, complexity and high cost is prohibitive for widespread commercial applications. Multifunctional reconfigurable antenna (MRA), with its capability to dynamically change antenna properties (e.g., frequency, radiation pattern and polarization) by adjusting its electrical properties has gained a lot of interest for future wireless networks. A multifunctional reconfigurable antenna array (MRAA) has been designed in [12] by creating a linear array of four identical MRA. This MRAA provides some benefits compared to traditional phased array by alleviating the inherent scan loss in standard antenna array and eliminating the need of expensive phase shifter circuitry and RF-chains for beam steering in certain plane. While a traditional phased array is constrained to steer its main beam only in the plane which contains the line on which the centers of the array elements lie, the MRAA presented in this dissertation is capable of steering its beam in both the steering plane of phased array and in the plane perpendicular to it. Moreover, it potentially provides higher gain and is capable of polarization configurability. However, this MRAA has a limited beam steering capability. The steering angle of the main beam is limited to the steering angle of the individual antennas.

In this chapter, two different MRAA designs are presented: i) MRAA with identical elements and ii) Generic MRAA. The first MRAA is designed solely by creating linear array of four identical MRA units presented in Chapter 4. The second MRAA presented in this dissertation, comprises of a 4×1 linear patch antenna array of four equally spaced identical

elements and a reconfigurable parasitic surface, a grid of rectangular metallic pixels, placed above. The pixels are distributed evenly on the parasitic surface. Adjacent pixels are connected to each other by means of p-i-n diode switches which can be turned ON/OFF to reconfigure the geometry of the pixels surface in order to change the current distribution which enables the reconfigurablity of the radiation pattern. These MRAAs overcome the constraint of steering angle by optimizing the pixels size and inter-pixel distance to get good steering performance in the linear array.

6.2 Antenna Design and Simulation Results

The design of MRAAs presented is based on the MRA and broadband high gain antenna array designs presented in Chapters 4 and 5, respectively. The main novelty of this MRAA is its variable element factor, which is fixed for legacy antenna arrays, similar to phased array antennas. The design efforts is carried out by full-wave EM simulation tool, ANSYS HFSS. The interconnections between parasitic pixel elements are assumed initially as perfect short and perfect open. The main goal of this design effort is to start laying the foundation of a new class of antenna array, i.e., MRAA.

6.2.1 Design of MRAA with identical elements

A 4×1 linear array structure as shown in Fig. 6.1 is designed to reconfigure the main beam direction of the radiation pattern into three different directions pertaining to: $\theta \in \{-30^0, 0^0, 30^0\}$; $\phi = 90^0$ over $59 - 66$ GHz band. The antenna structure consists of three layers namely, the feed, driven antenna, and reconfigurable parasitic layers with substrate thicknesses of 525 μm, 260 μm and 500 μm, respectively. The bottom and middle layers which house the CPW-fed loop and driven patch antenna, respectively, are formed on quartz substrates ($\varepsilon_r = 3.9$, $\tan\delta = 0.0002$ at 60 GHz). The CPW-fed loop couples the EM energy to the patch antenna, which results in a broad BW. The top layer is made out of low cost pyrex material ($\varepsilon_r = 4.9$, $\tan\delta = 0.01$ at 60 GHz) which is thinned down to 100 μm using standard clean room wet-chemical etch process. The upper surface of this layer has 3×3 metallic rectangular shaped pixels for each antenna element of 800 μm $\times$ 800 μm

size. The adjacent pixel surfaces are connected by p-i-n diodes. Inter-pixel distance 400 μm of the rectangular pixel grid on the parasitic surface is optimized to get better steering of the main beam. The four elements formed by placing identical patch antenna at inter element spacing of 0.7λ where λ is measured in free-space. The inter element distance of the individual element is optimized to reduce mutual coupling and get highest possible gain in broadside direction. The antenna array is fed by corporate feed network to ensure the elements are fed with equal phase. The optimized design parameters of the patch element, CPW-fed loop, and the reconfigurable parasitic layer which are obtained by full-wave EM simulations are provided in Table 6.1.

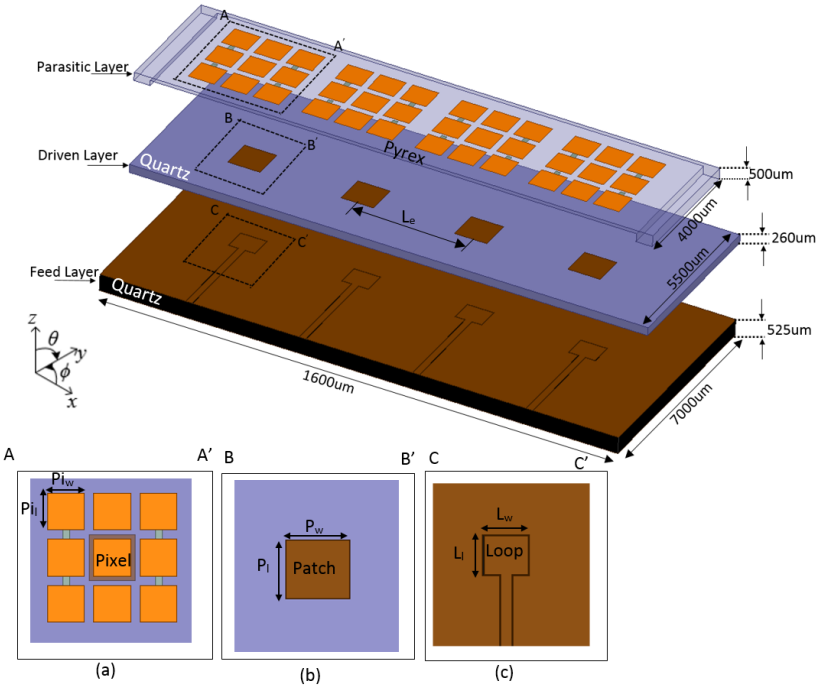

Fig. 6.1: Schematic of 3-D structure of 4×1 MRAA, (a) Enlarged A-A′, (b) Enlarged B-B′(c) Enlarged C-C′.

Table 6.1: Design parameters(dimensions are in mm).

Pi_l	0.8	P_l	1	L_l	0.7	L_e	$0.7\lambda_0$
Pi_w	0.8	P_w	1	L_w	0.8		

6.2.2 Simulation Results and Characterization of MRAA with identical elements

The top view of the MRAA showing switch locations are depicted in Fig. 6.2. A multi-objective genetic algorithm optimization [44] in conjunction with full-wave analysis is used to design the reconfigurable parasitic surface. Results indicate that only sixteen out of forty eight interconnections need to be controlled in order to achieve targeted three beam steering directions pertaining to: $\theta \in \{-30^0, 0^0, 30^0\}$; $\phi = 90^0$ over $59-66$ GHz band. The corresponding optimized switch configurations are given in Table 6.2.

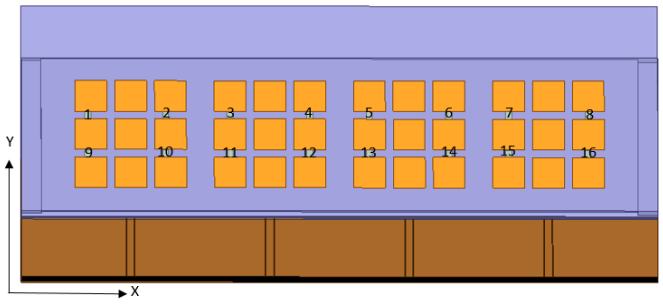

Fig. 6.2: Top view MRAA with identical antennas.

The simulated reflection coefficients for all the three modes of operation $\theta \in \{-30^0, 0^0, 30^0\}$; $\phi = 90^0$ are given in Fig. 6.3. The intersection of three individual reflection coefficients indicate a common BW of 10 GHz covering $57-67$ GHz band. The total realized gain patterns in $\phi = 90^0$ $(y-z)$ plane corresponding to each mode of operation at 60 GHz are shown in Fig. 6.4. The maximum realized gain values in the steered beam directions are all above ~ 13 dBi. The realized gain values for all three directions in $\phi = 90^0$ of operation over the entire $57-64$ GHz band are in the range $\sim 13-13.7$ dB as shown in Fig. 6.5.

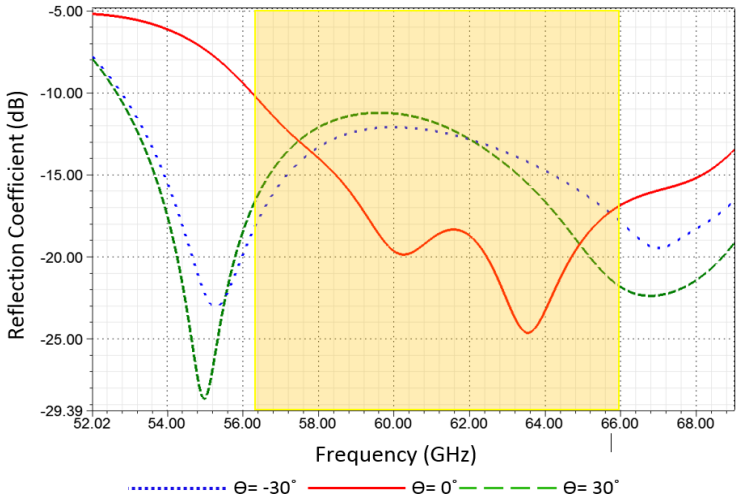

Fig. 6.3: The simulated reflection coefficient of the MRAA in $\phi = 90^0$ $(y - z)$ plane.

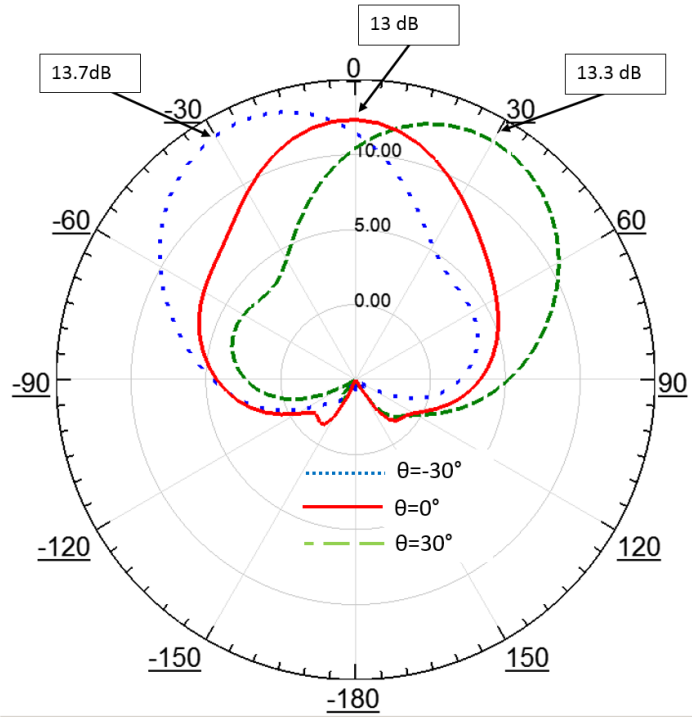

Fig. 6.4: Simulated total realized gain plots of the MRAA in $\phi = 90^0$ $(y - z)$ plane.

Table 6.2: The switch status corresponding to three beam steering directions of the 60 GHz MRAA obtained from GA's result(0 and 1 correspond to OFF and ON states, respectively).

Switch Number	1	2	3	4	5	6	7	8	9	10	11	12	13	14	15	16
$\phi = 90^0, \theta = 0^0$	0	0	0	0	0	0	0	0	0	0	0	0	0	0	0	0
$\phi = 90^0, \theta = -30^0$	1	1	1	1	1	1	1	1	0	0	0	0	0	0	0	0
$\phi = 90^0, \theta = 30^0$	0	0	0	0	0	0	0	0	1	1	1	1	1	1	1	1

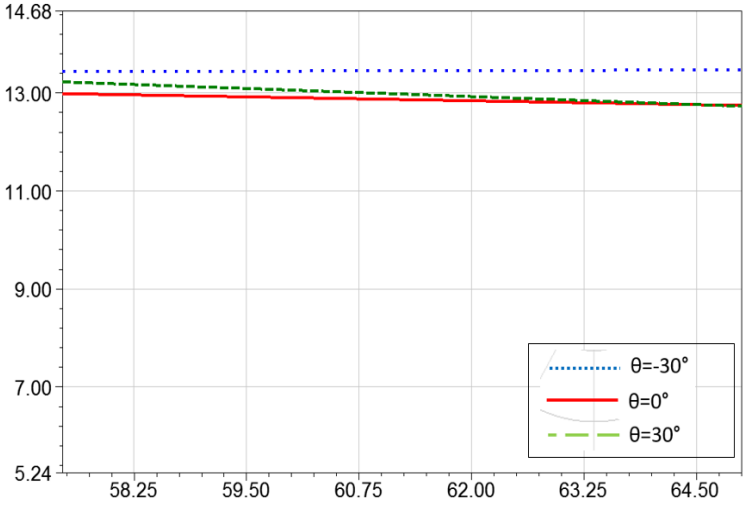

Fig. 6.5: Simulated realized gain values over $59 - 64$ GHz band for three beam-steering directions $\theta \in \{-30^0, 0^0, 30^0\}$; $\phi = 90^0$ $(y - z)$ plane.

6.2.3 Design of Generic MRAA

A generic 4×1 linear array structure is formed by placing identical patch antenna at inter element spacing of 0.7λ. The inter element distance of the individual element is optimized to reduce mutual coupling and get highest possible gain in broadside direction. The antenna array is fed by corporate feed network to ensure the elements are fed with equal phase. The feed network and coplanar waveguide (CPW) loop are placed on a quartz layer of 525 μm thickness. The driven patches are placed on a separate quartz layer of 260 μm thickness which is located on top of the feed structure. A parasitic layer formed with pyrex of 500 μm thickness is used to support a 3×11 grid of rectangular metallic pixels of size 800 $\mu m \times 800$ μm. The adjacent pixel surfaces are connected by p-i-n diodes. Inter pixel distance 500 μm of the rectangular pixel grid on the parasitic surface is optimized to get better steering of the main beam. This MRAA is generic in the sense of pixel layer geometry

and interconnections. This generic MRAA essentially has the same active antenna and feed network layer (Fig. 6.1). Generic MRAA differs from MRAA with identical elements only in terms of parasitic layer geometry. The geometry of the parasitic layer of this MRAA is shown in Fig. 6.6 and discussed in detail in the section subsection.

6.2.4 Simulation Results and Characterization of Generic MRAA

The top view of the generic MRAA showing switch locations are depicted in Fig. 6.6. A multi-objective genetic algorithm optimization [44] in conjunction with full-wave analysis is used to design the reconfigurable parasitic surface. Results indicate that only sixteen out of fifty-two interconnections need to be controlled to control the tilt angle. This design is capable of tilting the beam into $\theta \in \{-50^0, 0^0, 50^0\}$; $\phi = 90^0$ over $59 - 66$ GHz band. The corresponding optimized switch configurations are given in Table 6.3.

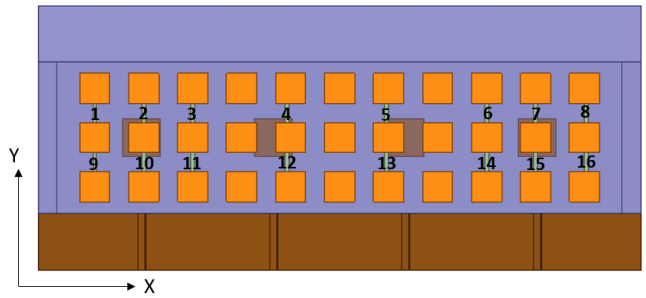

Fig. 6.6: Top view of generic MRAA. 1,2...16 denote switches location.

The simulated reflection coefficients for all the three modes of operation $\theta \in \{-50^0, 0^0, 50^0\}$; $\phi = 90^0$ are given in Fig. 6.7. The intersection of three individual reflection coefficients indicate a common BW of 10 GHz covering $57 - 67$ GHz band. The total realized gain patterns in $\phi = 90^0$ $(y - z)$ plane corresponding to each mode of operation at 60 GHz are shown in Fig. 6.8. The maximum realized gain values in the steered beam directions are all above ~ 13 dBi. The realized gain values for all three directions in $\phi = 90^0$ of operation over the entire $59 - 66$ GHz band are in the range $\sim 11.7 - 12.7$ dB as shown in Fig. 6.9.

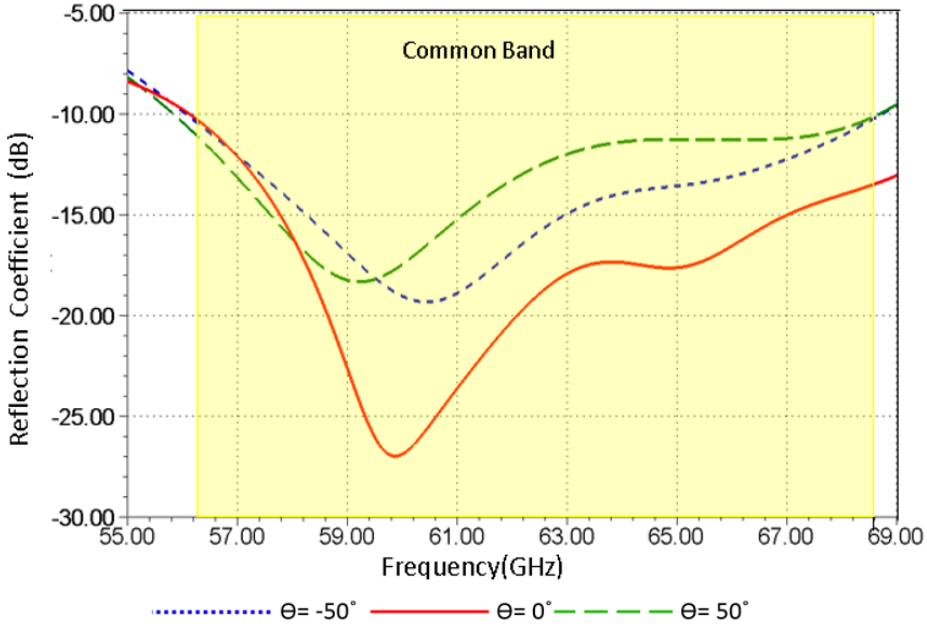

Fig. 6.7: The simulated reflection coefficient of the MRAA in $\phi = 90^0$ $(y - z)$ plane.

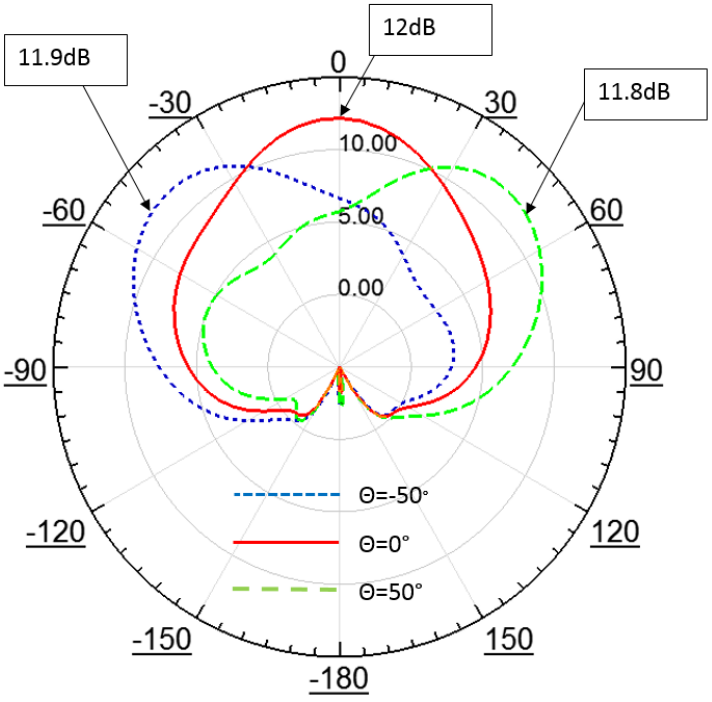

Fig. 6.8: The simulated total realized gain plots of the MRAA in $\phi = 90^0$ $(y - z)$ plane.

Table 6.3: The switch status corresponding to three beam steering directions of the 60 GHz MRAA obtained from GA's result(0 and 1 correspond to OFF and ON states, respectively).

Switch Number	1	2	3	4	5	6	7	8	9	10	11	12	13	14	15	16
$\phi = 90^0, \theta = 0^0$	0	0	0	0	0	0	0	0	0	0	0	0	0	0	0	0
$\phi = 90^0, \theta = -50^0$	1	1	1	1	1	1	1	1	0	0	0	0	0	0	0	0
$\phi = 90^0, \theta = 50^0$	0	0	0	0	0	0	0	0	1	1	1	1	1	1	1	1

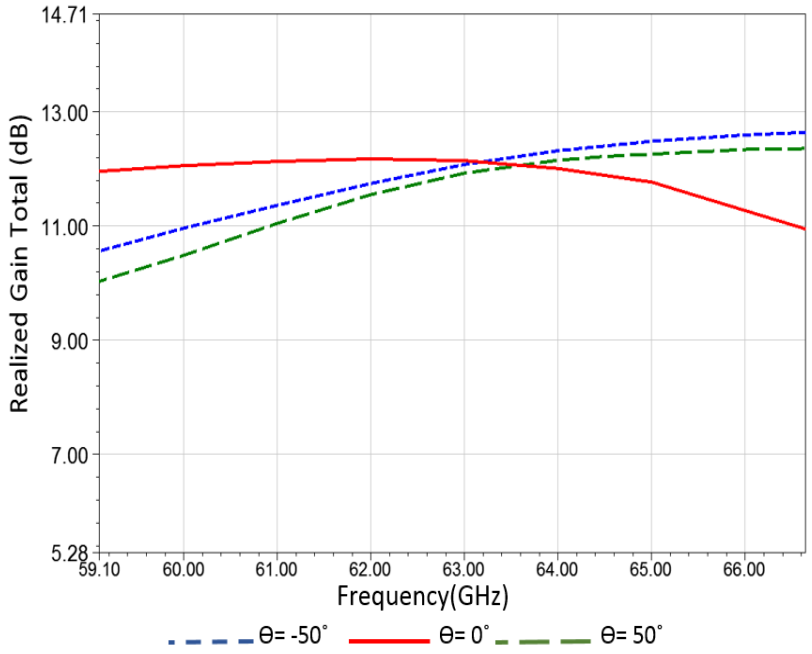

Fig. 6.9: The simulated realized gain values over $59 - 66$ GHz band for three beam-steering directions $\theta \in \{-50^0, 0^0, 50^0\}$; $\phi = 90^0$ $(y - z)$ plane.

6.3 Working Mechanism

In a typical antenna array, identical antenna elements are used which can be individually controlled in phase and magnitude. Far field radiation pattern of a typical linear antenna array, $F(\theta, \phi)$, can be found by using the principle of pattern multiplication, which is given in [50],

$$F(\theta, \phi) = E_a(\theta, \phi) \times F_a(\theta, \phi). \tag{6.1}$$

Here, $E_a(\theta, \phi)$ is the normalized pattern of the individual antenna, also known as element factor and $F_a(\theta, \phi)$ is normalized array factor. For a uniform amplitude excitation, it can

be expressed as

$$F_a(\theta,\phi) = \frac{\sin[\frac{N\pi d}{\lambda_0} \times (\sin\theta - \sin\theta_0)]}{N\sin[\frac{\pi d}{\lambda_0} \times (\sin\theta - \sin\theta_0)]}. \tag{6.2}$$

Here, N is the total number of array elements and $\theta = \theta_0$ is the beam steering direction in $y-z$ plane. Beam steering in a phased array is achieved by feeding antenna array elements with complex excitation with uniform amplitude of a_0 and progressive phase shift from element to element, $k_0 d sin\theta_0$. The complex excitations are given by

$$a_n = a_0 e^{(-jk_0 nd\sin\theta_0)} \tag{6.3}$$

where $n = 0, 1, 2, 3, ...$ and $k_0 = \frac{2\pi}{\lambda_0}$ is the free space wave number at center frequency. It is apparent from the above equations that radiation pattern of a traditional phased array is mainly controlled by the array factor. Since element factor is fixed by initial design, it does not play any role in beam steering. In the MRAA proposed in this dissertation, individual elements will not have identical radiation pattern as the pixel surface is not identical for every element. For a linear antenna array with non-identical element patterns, the antenna array pattern can be written as

$$F_a(\theta,\phi) = E_1(\theta,\phi) + E_2(\theta,\phi)e^{j\psi} + E_3(\theta,\phi)e^{j2\psi} + ... + E_{N-1}(\theta,\phi)e^{(j(N-1)\psi)} \tag{6.4}$$

where $\psi = kdcos\theta + \beta$ and $E_1, E_2....E_{N-1}$ are individual element factors. The parasitic surface geometry of the MRAA is reconfigured by connecting or disconnecting the adjacent pixels of this surface. Change of parasitic surface geometry results in different reactive loading for individual elements. According to the theory of reactively controlled directive array by R.F. Harrington [53], the main beam direction of the driven antenna can be directed into a desired direction by reactive loading of the parasitic elements. Hence, the reactive loading of the driven individual elements produces non-identical radiation patterns which add up according to above Equation (6.4) to form a desired radiation pattern of the antenna array. In summary, the individual radiation patterns of the non-identical elements are changed in such a way that they form a desired array pattern when they add up.

6.4 Comparison of MRAA with Identical Elements and Generic MRAA

This section presents the comparison of beam steering angle of MRAA with identical element and generic MRAA for two different modes. Mode-1 refers to the MRAA mode with tilt angle in positive theta direction ($+\theta$) and mode-2 refers to the MRAA mode with tilt angle in negative theta direction ($-\theta$). The radiation patterns for MRAA with identical elements and generic MRAA for mode-1 and mode-2 are given in Fig. 6.10 and Fig. 6.11 respectively. The results shows that, the generic MRAA has maximum gain in $y-z$ plane for $\theta = \pm 50^0$ whereas MRAA with identical element has maximum gain in $y-z$ plane for $\theta = \pm 30^0$. It becomes evident from the comparison that the generic MRAA has more tilt compared to MRAA with identical elements which indicates that non-identical elements patterns are adding up according to Equation (6.4), resulting in an array pattern that overcomes the beam steering limitation of the MRAA with identical elements.

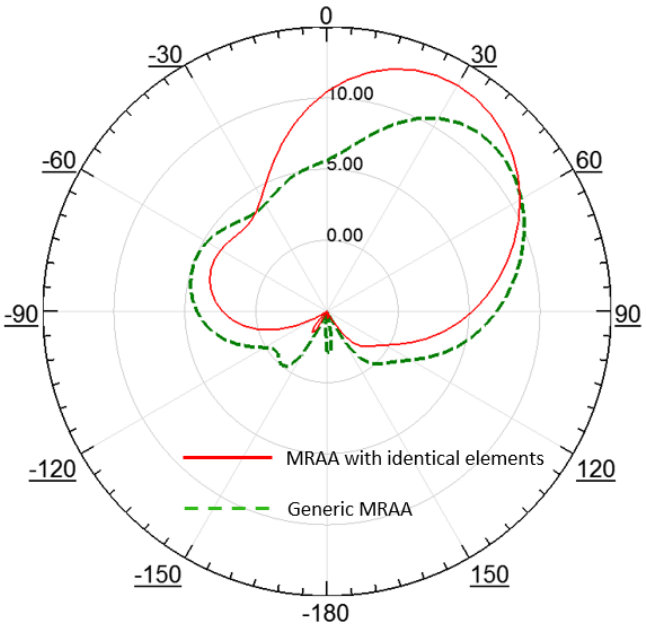

Fig. 6.10: The simulated maximum beam tilt direction of generic MRAA and MRAA with identical elements in $\phi = 90^0$ $(y-z)$ plane for mode-1 .

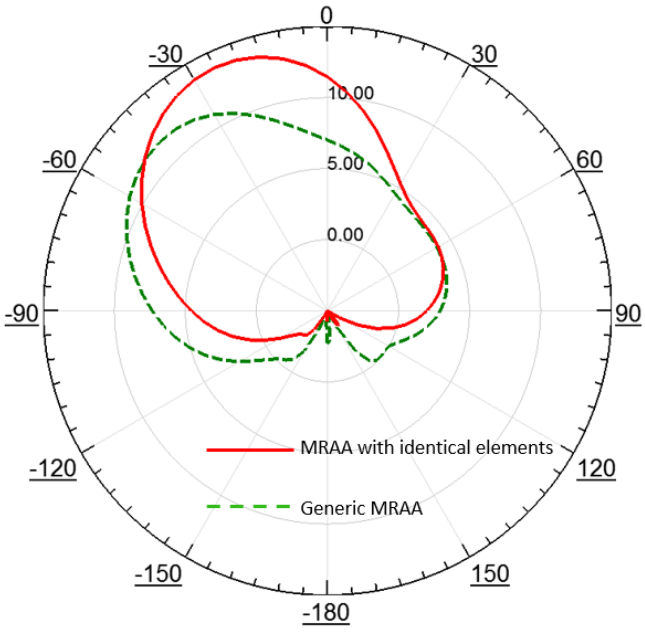

Fig. 6.11: The simulated maximum beam tilt direction of generic MRAA and MRAA with identical elements in $\phi = 90^0$ $(y - z)$ plane for mode-2.

6.5 Conclusion

In this chapter initial efforts towards developing a new class of antenna array called MRAA that is capable of working at mm-wave have been presented. The main goal was to facilitate beam steering at mm-wave communication for future wireless networks with a reduction in complexity from legacy phase antenna array. Simulation results show that the generic MRAA structure can provide greater beam steering compared to MRAA with identical elements. This novel generic MRAA is promising to have great benefits which needs to be exploited. The performance of the generic MRAA can be improved by further optimization of the pixel layer geometry and pixel number, which is left as a future work.

CHAPTER 7
INVESTIGATION AND SIMULATIONS OF VARIOUS SWITCH TECHNOLOGIES FOR MRA INTEGRATION

7.1 Introduction

The designs and ongoing micro-fabrication efforts consider initially perfect short and perfect open for interconnections between adjacent pixels. However, for a real life dynamic prototype, a proper switching technology should be used. There are various competing switch technologies that can be used for the MRAs designed. Among others, micro-fabrication compatibility, cost, RF performance and monolithic integration are the main factors to consider in adapting the most proper technology. To this end, we will investigate p-i-n diodes, RF transistors and smart material based switches such as vanadium oxide (VO_2). Although we have plenty of experiences with p-i-n diodes and RF transistors at lower frequencies ($\leq$ 15 GHz), at frequencies above 30 GHz the switching characteristics of p-i-n diodes and RF transistors are not well known. Degraded RF performances and integration challenges due to exceedingly small dimensions are the main issues to tackle at high frequencies. Recently, we started exploring VO_2 smart material of which conductivity can be varied (from good conductor to weak conductor) in response to an applied thermal energy. This material is also advantageous in terms of micro-fabrication compatibility which enables its monolithic integration with parasitic pixel segments. We intend to investigate all these switching technologies through simulation and measurements, with the goal of determining pros and cons of each switching technologies; which will ultimately enable us to choose the most optimum one.

7.2 RF Transistors

Field-effect transistor (FET) is a semiconductor device which depends on an electric

field to control the conductivity of a channel in the semiconductor material. The current between source and drain connections is controlled by a voltage applied between the gate and source. FET switches are stable and reliable due to good control of the drain-to-source channel resistance and high ON/OFF current ratios. The application of a reverse-biasing voltage between gate and source causes the depletion region at that junction to expand, thereby, "pinching-off" the channel between source and drain through which the controlled current travels. In the OFF state, the conduction channel is depleted (pinched-off), which causes the FET to exhibit very high resistance, mechanism which provides good isolation at low frequencies. The isolation of FET switches degrades at higher frequencies due to the effect of drain-to source capacitance (CDS). For example a GaAs FET has the reactance X_C of the CDS at 10 GHz about 320 Ω which can give an equivalent of about 10 dB drain-to-source isolation, which is not sufficient to satisfy the isolation performance. There is generally a trade off between insertion loss and isolation in the FET geometry and profile. The allowable geometry and profile are determined by the performance requirements of the switch. However, when the frequency becomes higher, typically above 10 GHz, the FET off state capacitance increases resulting in a lower impedance, and this degrades the isolation of the switch [54]. This means that the switch cannot have both low loss and high isolation in the high frequency region. Resonance is often used to obtain high isolation between the FET drain and source [55, 56]. Blackwell et al. also had an approach in which they used specific device fabrication techniques to reduce the off-state capacitance [57].

7.3 P-I-N Diodes

The geometry of the parasitic surface can also be configured by p-i-n diode switches. In this case, the components in the gaps between adjacent pixels on the upper face of parasitic layer consist of: the interconnecting p-i-n diodes, DC-block capacitors, and RF choke inductors in parallel to the p-i-n diodes. Four different kinds of lumped components are used on the parasitic layer as shown in Fig. 7.1. 1) P-I-N diode switches are used in between pixels. Metallic pixels are connected/disconnected by switching ON/OFF the p-i-n diode switches to dynamically change the geometry of the parasitic surface, which in turn

change the current distribution, and thus antenna characteristics. 2) Inductors are placed along the DC bias lines as RF chokes. The RF choke is a circuit element designed to present high impedance to RF energy while offering minimal resistance to direct current. Usually the choke reactance shall be greater than 500 Ω at working frequency. The choke reactance is given by:

$$X_L = 2\pi FL \tag{7.1}$$

The self resonant frequency (SRF) of the RF choke is chosen such that RF chokes would appear as high impedance in 802.11ad band to minimize the current on the bias lines, thereby minimizing the mutual coupling effects of the bias lines on the antenna performance. 3) Inductors are also placed in between all pixels. In this manner, all the pixels can be DC grounded together to provide ground for DC biasing purpose. The SRF of these inductors was chosen to be the same value as RF chokes to keep the high RF impedance between pixels. 4) DC block capacitors are used to properly bias the p-i-n diode switches [58]. In general DC blocking capacitor shall behave like a short at working frequency. Calculating the reluctance in ohms of DC blocking capacitor for minimum value at working frequency is done as:

$$X_C = \frac{1}{2\pi FC} \tag{7.2}$$

The DC biasing scheme of the p-i-n switch is shown in Fig. 7.2. It can be seen that lumped components mentioned above are required to properly bias the p-i-n diode. Typically, 1 V DC power supply on the p-i-n diode would be sufficient to turn on the switch, while 0 V will keep the switch in OFF status. The equivalent circuit models of these lumped components are obtained by using their scattering parameters provided by the manufacturers. These equivalent circuit models are used in the design of the MRAs by full-wave HFSS analyses. The theory behind the working mechanism of a parasitic pixel layer based pattern reconfigurable antenna is explained by Yuan et al [27].

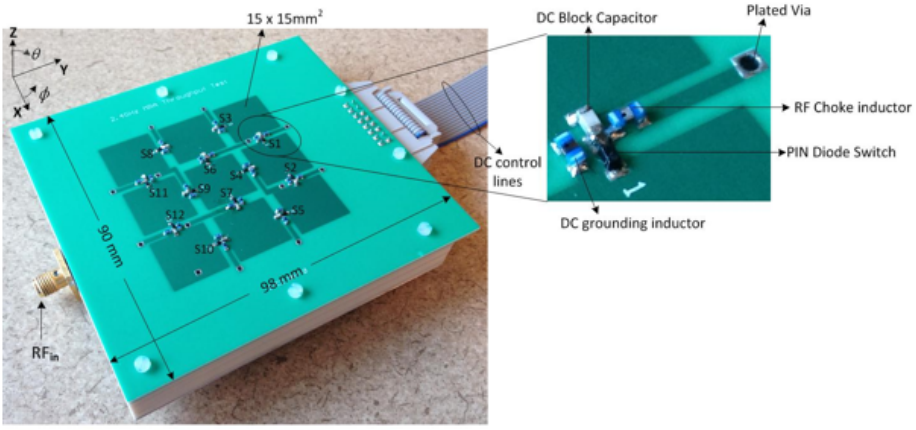

Fig. 7.1: P-I-N diode switch and integrated lumped components on the parasitic layer of a MRA prototype.

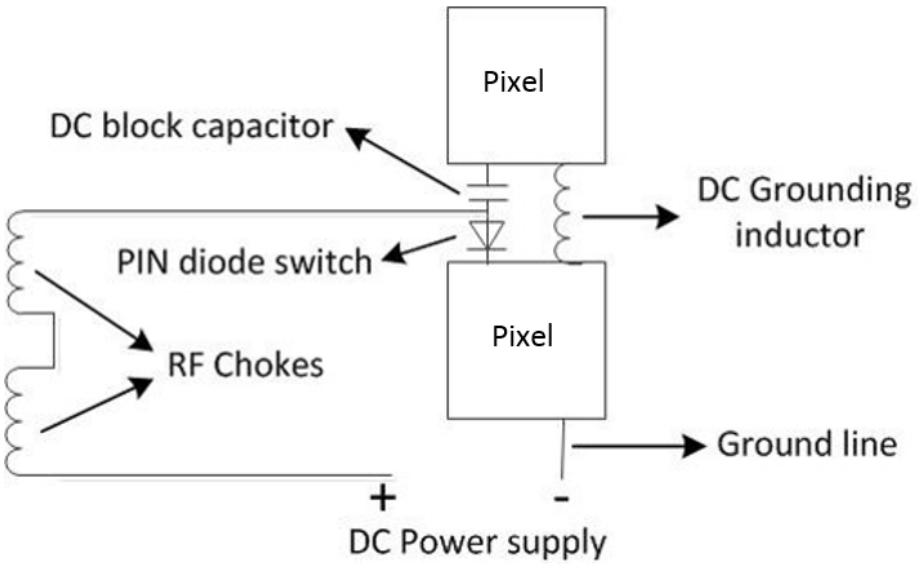

Fig. 7.2: DC biasing scheme of a p-i-n diode switch.

The DC block capacitor is modeled as a series LC resonant circuit in HFSS using

$$SRF = \frac{1}{2\pi\sqrt{LC}} \tag{7.3}$$

where L represents the lead inductance of the SMD, C is the value of the capacitance chosen, and SRF is the self-resonant frequency obtained from datasheet. From Equation (7.3) L is calculated and it is verified that this series resonance provides sufficiently low impedance to RF path between pixels in the frequency band of interest. The RF choke inductor, delimits the bias line metallization to avoid deleterious coupling effects on targeted antenna performances. This inductor is modeled as a parallel LC resonant circuit using Equation (7.3) with its C calculated from given in the datasheet. Here, C accounts for the parasitic capacitance between the terminals of inductor.

7.4 Smart Material

Smart materials can be used in electrical switches, in addition to their use in non-volatile memory [59, 60] and optical storage [61, 62]. One advantage of using phase change materials is that they do not require energy to maintain either the ON (crystalline state) or OFF (amorphous state) state thus reducing power consumption in any application. This work emphasizes the development of smart materials for switches with low resistance in the ON state. One of the applications for switches with low ON state resistance is in radio frequency (RF) circuits. Vanadium dioxide (VO_2) is currently considered as one of the most promising materials for oxide electronics [63]. VO_2 phase change materials have been identified in this work as materials with which it is possible to achieve a low ON state resistance and large dynamic range and that could be suitable for RF circuit applications. VO_2 has a constant and stable metal to insulator transitions temperature at 68^0C, and a resistivity superior ratio (three to four order of magnitude) between metallic and insulator phases compared with the other forms of vanadium oxides [62,64]. The resistance of VO_2 has been measured in different kinds of experiments. First, the resistance of VO_2 was measured at hydrostatic pressures up to 2 GPa and room temperature using electric-field-induced

resistance switching of VO_2 planar-type junctions [65]. Second, the VO_2 was fabricated in number of parallel strip patterns in the varistor, and the resistance of the VO_2 flake has been measured [66]. Third, the resistance of the VO_2 was measured by VO_2 flake-based RF shunt resonator, and the VO_2 flake was deposited as shunt resistance in this device [67]. An important parameter for such two terminal switches is the switching speed between the insulating and metallic state, which could provide information on both application potential and the transition mechanism. It was reported that switching speed of VO_2 devices is limited to several nanoseconds either due to the test structure or measurement setup limitations . The demonstrated fastest switching speed (from electrical measurements) is $\sim$ 5 ns for planar devices, and $\sim$ 170 ns for out-of-plane devices. Although out-of-plane metal-VO_2-metal structures are desirable for memory devices, direct growth on semiconducting substrates such as silicon limits the switching speed measurements due to the additional series resistance [68]. VO_2 flake was designed to connect adjacent pixels. The VO_2 flake acts like an insulator making the device OFF (resistivity $5 \times 10^{-2}\Omega - m$). At temperatures above 68^0C, the VO_2 flake becomes a conductor (resistivity $2.5 \times 10^{-6}\Omega - m$), allowing current signal to go through. Smart material switches can be used on the antenna parasitic layer as shown in Fig. 7.3.

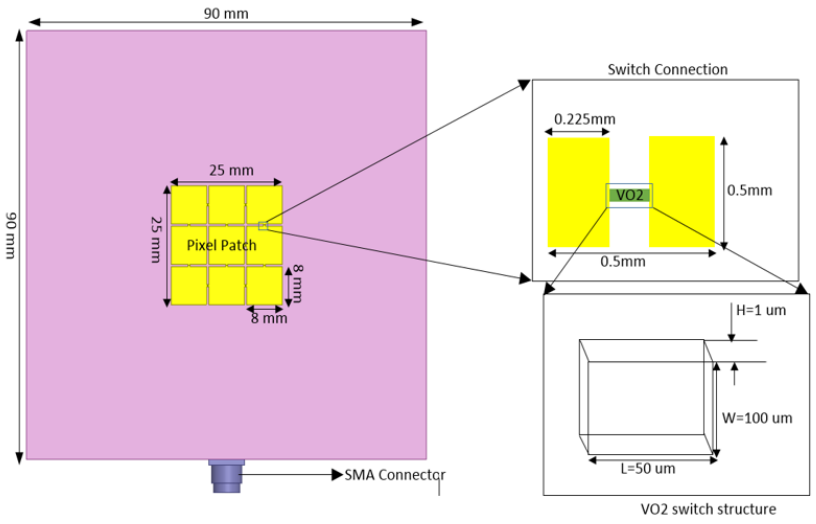

Fig. 7.3: Smart materiel switch.

7.5 Comparison of Simulation Results

To compare the switching characteristics of smart material VO_2 with a traditional p-i-n diode (MA4AGBL912), a simple transmission line with an interconnection is designed in HFSS. Fig. 7.4 shows the transmission line used to compare the switching performances. The result for the transmission line at ON state have presented in Fig. 7.5. Comparing the simulated results, it is clear that smart material has less insertion loss compared to p-i-n diode across broad frequency band at ON state. The isolation for p-i-n diode and smart material switch is given in Fig. 7.6 shows that smart material has very good isolation (< 23 dB) compared to p-i-n diode (> 23 dB) in OFF state.

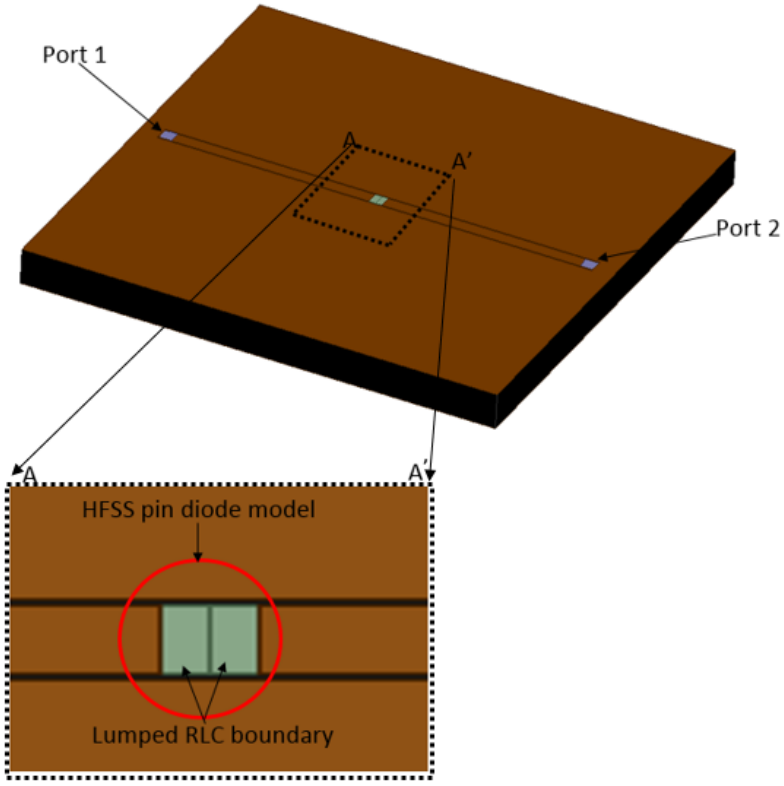

Fig. 7.4: The simulated p-i-n switch.

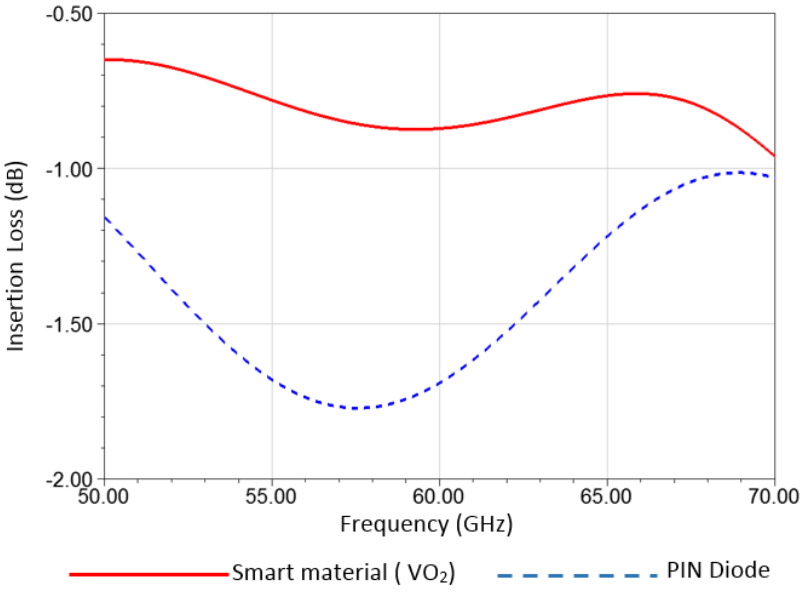

Fig. 7.5: Simulated transmission line p-i-n and VO_2 switch at ON state.

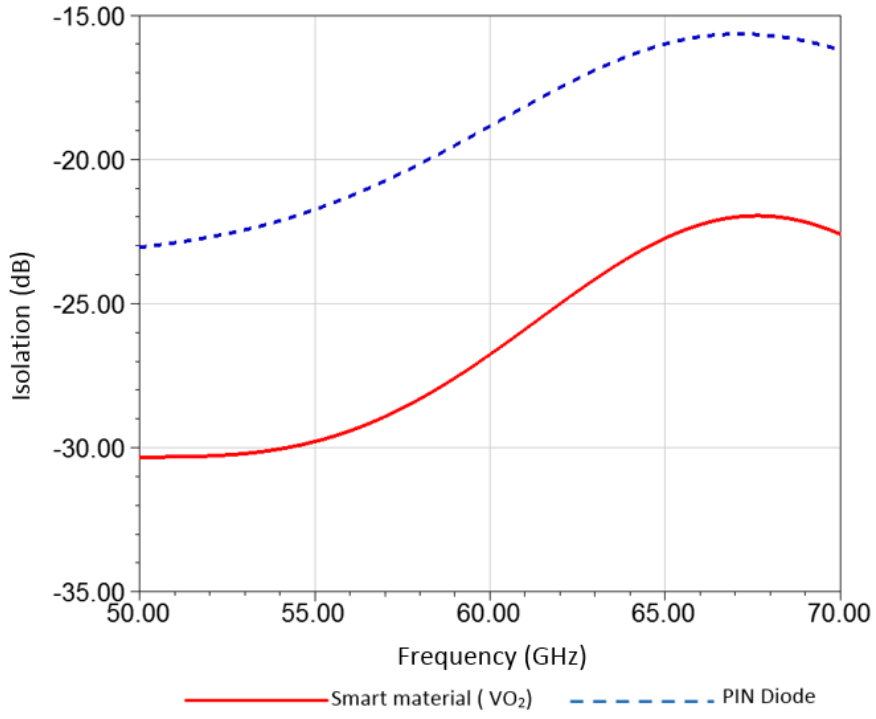

Fig. 7.6: Simulated transmission line p-i-n and VO_2 switch at OFF state.

7.6 Conclusion

In this chapter, performance comparison of p-i-n diode and smart material based switches have been presented. Insertion loss and isolation comparison shows that smart material, e.g., VO_2 has less insertion loss and better isolation compared to a typical p-i-n diode. Hence, smart material with its ease of integration and better performance has a great potential to be a candidate for MRA and MRAA switching. Specially, due to its ability to perform across a broad BW, even at mm-wave, VO_2 can be an excellent choice for dynamic configuration of pixel layer. Smart materials are still under investigation and have been receiving a lot of attention recently. So, the state-of-the-art of this switching technology still has a lot of research opportunities. The results presented here show a lot of promise. However, this simulation results have to be verified by fabrication and measurements which is left as a future work.

CHAPTER 8

CONCLUSIONS AND FUTURE WORK

This dissertation presents multiple antennas operating at 60 GHz band. The design and micro-fabrication of a legacy patch antenna operating at $57-66$ GHz band have been presented in Chapter 3. The simulated impedance characteristics and radiation pattern show $\sim 15\%$ bandwidth with a realized gain value of ~ 8.5 dB in the broadside direction over the entire band. An MRA with beam steering capability based on the principle of parasitic tuning is presented in Chapter 4. The simulation results for different operational modes indicates a reasonable realized gain around 7 dBi covering 59-64 GHz band. This MRA prototype capable of dynamic beam steering was later used as a building block to design MRAA. A 2×8 patch antenna planar array operating in the IEEE 802.11ad frequency band (57-66 GHz) is presented in Chapter 5. Simulation results indicate relatively constant gain values ($17-19.3$ dB) over $57-65$ GHz band, which makes the designed array a strong candidate for multi-gigabit applications. In Chapter 6, two different 4×1 MRAA designs are presented: MRAA with identical elements and generic MRAA. The main goal was to facilitate beam steering at mm-wave communication for future wireless networks with a reduction in complexity from legacy phase antenna array. Simulation results show that the generic MRAA structure can provide greater beam steering compared to MRAA with identical elements. This novel generic MRAA is promising to have great benefits which can be exploited further to make this design a strong candidate to be an integral part of the air interface in 5G and beyond wireless network. Finally, at Chapter 7, switching characteristics of p-i-n diode and smart material based switches have been investigated. Comparison of insertion loss and isolation demonstrates that smart material, e.g., VO_2 based switching can be superior to legacy p-i-n diodes, thus showing a great promise to be a strong candidate for switching technologies of MRA and MRAA.

The measurements of the antennas which are presented in this dissertation is already

underway. Generic MRAA prototype suffers from some gain degradation which can be thought as the cost of greater beam tilt and smaller number of pixel interconnection. However, there is room to improve the performance of generic MRAA by optimizing the pixel layer geometry. This joint optimization problem is left as a future work. In addition, smart material based switching technique for MRA and MRAA can be further investigated through micro-fabrication, measurement and characterization. In addition, possible use of other materials for MRA and MRAA smart material based switching at high frequencies can be a promising future research direction.

REFERENCES

[1] T. S. Rappaport, W. Roh, and K. Cheun, "Mobile's millimeter-wave makeover," *IEEE Spectrum*, vol. 51, no. 9, pp. 34–58, Sept 2014.

[2] J. G. Andrews, S. Buzzi, W. Choi, S. V. Hanly, A. Lozano, A. C. K. Soong, and J. C. Zhang, "What will 5g be?" *IEEE Journal on Selected Areas in Communications*, vol. 32, no. 6, pp. 1065–1082, June 2014.

[3] R. Daniels and R. Heath, "60 ghz wireless communications: emerging requirements and design recommendations," *Vehicular Technology Magazine, IEEE*, vol. 2, no. 3, pp. 41–50, Sept 2007.

[4] S. S. N., D. Dash, H. E. Madi, and G. Gopalakrishnan, "WiGig and IEEE 802.11ad - For multi-gigabyte-per-second WPAN and WLAN," p. 24, 2012. [Online]. Available: http://arxiv.org/abs/1211.7356

[5] C. Hansen, "Wigig: Multi-gigabit wireless communications in the 60 ghz band," *Wireless Communications, IEEE*, vol. 18, no. 6, pp. 6–7, December 2011.

[6] W.-F. Alliance, "WiGig and the future of seamless connectivity," 2013.

[7] H. V. Hunerli, H. Mopidevi, E. Cagatay, M. Imbert, J. Romeu, L. Jofre, B. A. Cetiner, and N. Biyikli, "Three dimensional microfabricated broadband patch and multifunction reconfigurable antennae for 60 GHz applications," in *2015 9th European Conference on Antennas and Propagation (EuCAP)*. IEEE, 2015, pp. 1–5. [Online]. Available: http://ieeexplore.ieee.org/xpls/abs_all.jsp?arnumber=7228902

[8] R. J. Mailloux, "Phased array antenna handbook," *Boston, MA: Artech House.*, 1994.

[9] K. Araki, A. Tanaka, and E. Matsumura, "Wide scanning phased array antenna design in ka band," *IEE Proceedings - Microwaves, Antennas and Propagation*, vol. 150, no. 5, pp. 379–84–, Oct 2003.

[10] X. Ding, B.-Z. Wang, and G.-Q. He, "Research on a millimeter-wave phased array with wide-angle scanning performance," *IEEE Transactions on Antennas and Propagation*, vol. 61, no. 10, pp. 5319–5324, Oct 2013.

[11] T.-Y. Yun, C. Wang, P. Zepeda, C. T. Rodenbeck, M. R. Coutant, M. yi Li, and K. Chang, "A 10- to 21-ghz, low-cost, multifrequency, and full-duplex phased-array antenna system," *IEEE Transactions on Antennas and Propagation*, vol. 50, no. 5, pp. 641–650, May 2002.

[12] Z. Li, D. Rodrigo, L. Jofre, and B. Cetiner, "A new class of antenna array with a reconfigurable element factor," *Antennas and Propagation, IEEE Transactions on*, vol. 61, no. 4, pp. 1947–1955, April 2013.

[13] A. Rashidian, D. M. Klymyshyn, M. T. Aligodarz, M. Boerner, and J. Mohr, "Su-8 resonator antenna," in *Antennas and Propagation Society International Symposium (APSURSI), 2010 IEEE*, July 2010, pp. 1–4.

[14] D. M. Klymyshyn, M. T. Aligodarz, A. Rashidian, M. Brner, and J. Mohr, "Photoresist-based resonator antenna array," in *Microwave Conference (GeMIC), 2011 German*, March 2011, pp. 1–4.

[15] K. Konstantinidis, A. P. Feresidis, Y. Tian, X. Shang, and M. J. Lancaster, "Micromachined terahertz fabry-perot cavity highly directive antennas," *IET Microwaves, Antennas Propagation*, vol. 9, no. 13, pp. 1436–1443, 2015.

[16] G. Gauthier, A. Courtay, and G. Rebeiz, "Microstrip antennas on synthesized low dielectric-constant substrates," *Antennas and Propagation, IEEE Transactions on*, vol. 45, no. 8, pp. 1310–1314, Aug 1997.

[17] H. Mopidevi, H. Hunerli, E. Cagatay, N. Biyikli, M. Imbert, J. Romeu, L. Jofre, and B. Cetiner, "Three-dimensional microfabricated broadband patch antenna for wigig applications," *Antennas and Wireless Propagation Letters, IEEE*, vol. 13, pp. 828–831, 2014.

[18] L. Wang, Y.-X. Guo, and W.-X. Sheng, "Wideband high-gain 60-ghz ltcc l-probe patch antenna array with a soft surface," *Antennas and Propagation, IEEE Transactions on*, vol. 61, no. 4, pp. 1802–1809, April 2013.

[19] S. B. Yeap, Z. N. Chen, and X. Qing, "Gain-enhanced 60-ghz ltcc antenna array with open air cavities," *Antennas and Propagation, IEEE Transactions on*, vol. 59, no. 9, pp. 3470–3473, Sept 2011.

[20] P. Smulders, H. Yang, and I. Akkermans, "On the design of low-cost 60-ghz radios for multigigabit-per-second transmission over short distances [topics in radio communications]," *Communications Magazine, IEEE*, vol. 45, no. 12, pp. 44–51, December 2007.

[21] A. Natarajan, S. K. Reynolds, M. D. Tsai, S. T. Nicolson, J. H. C. Zhan, D. G. Kam, D. Liu, Y. L. O. Huang, A. Valdes-Garcia, and B. A. Floyd, "A fully-integrated 16-element phased-array receiver in sige bicmos for 60-ghz communications," *IEEE Journal of Solid-State Circuits*, vol. 46, no. 5, pp. 1059–1075, May 2011.

[22] M. Kaynak, K. E. Ehwald, J. Drews, R. Scholz, F. Korndrfer, D. Knoll, B. Tillack, R. Barth, M. Birkholz, K. Schulz, Y. M. Sun, D. Wolansky, S. Leidich, S. Kurth, and Y. Gurbuz, "Beol embedded rf-mems switch for mm-wave applications," in *2009 IEEE International Electron Devices Meeting (IEDM)*, Dec 2009, pp. 1–4.

[23] L. L. Mercado, S. M. Kuo, T. Y. T. Lee, and L. Liu, "Mechanics-based solutions to rf mems switch stiction problem," *IEEE Transactions on Components and Packaging Technologies*, vol. 27, no. 3, pp. 560–567, Sept 2004.

[24] J. Chu, "Integrated microwave front-ends with avionics applications [book/software reviews]," *IEEE Microwave Magazine*, vol. 16, no. 4, pp. 130–132, May 2015.

[25] T. S. Rappaport, S. Sun, R. Mayzus, H. Zhao, Y. Azar, K. Wang, G. N. Wong, J. K. Schulz, M. Samimi, and F. Gutierrez, "Millimeter wave mobile communications for 5g cellular: It will work!" *IEEE Access*, vol. 1, pp. 335–349, 2013.

[26] T. Rappaport, J. Murdock, and F. Gutierrez, "State of the art in 60-ghz integrated circuits and systems for wireless communications," *Proceedings of the IEEE*, vol. 99, no. 8, pp. 1390–1436, Aug 2011.

[27] X. Yuan, Z. Li, D. Rodrigo, H. S. Mopidevi, O. Kaynar, L. Jofre, and B. A. Cetiner, "A parasitic layer-based reconfigurable antenna design by multi-objective optimization," *IEEE Transactions on Antennas and Propagation*, vol. 60, no. 6, pp. 2690–2701, June 2012.

[28] Y. Zhang, M. Sun, K. Chua, L. Wai, D. Liu, and B. Gaucher, "Antenna-in-Package in LTCC for 60-GHz Radio," in *International Workshop on Antenna Technology: Small and Smart Antennas Metamaterials and Applications, 2007. IWAT '07.*, vol. 1, no. 1, 2007, pp. 279–282. [Online]. Available: http://ieeexplore.ieee.org/xpls/abs_all.jsp?arnumber=4227445

[29] S. Wi, Y. Sun, and I. Song, "Package-level integrated antennas based on LTCC technology," *Antennas and Propagation, IEEE Transactions on*, 2006. [Online]. Available: http://ieeexplore.ieee.org/xpls/abs_all.jsp?arnumber=1668292

[30] S. Seok, N. Rolland, and P. A. Rolland, "Millimeter-wave quarter-wave patch antenna on benzocyclobutene polymer," in *Microwave Conference, 2008. EuMC 2008. 38th European*, Oct 2008, pp. 1018–1021.

[31] H. V. Hunerli, H. Mopidevi, E. Cagatay, M. Imbert, J. Romeu, L. Jofre, B. A. Cetiner, and N. Biyikli, "Three dimensional microfabricated broadband patch and multifunction reconfigurable antennae for 60 ghz applications," in *2015 9th European Conference on Antennas and Propagation (EuCAP)*, May 2015, pp. 1–5.

[32] T. Itoh, "Overview of quasi-planar transmission lines," *IEEE Transactions on Microwave Theory and Techniques*, vol. 37, no. 2, pp. 275–280, Feb 1989.

[33] A. Lamminen, J. Saily, and A. Vimpari, "60-ghz patch antennas and arrays on ltcc with embedded-cavity substrates," *Antennas and Propagation, IEEE Transactions on*, vol. 56, no. 9, pp. 2865–2874, Sept 2008.

[34] V. K. Singh, "Ka-band micromachined microstrip patch antenna," *IET Microwaves, Antennas Propagation*, vol. 4, no. 3, pp. 316–323, March 2010.

[35] A. Panther, A. Petosa, M. G. Stubbs, and K. Kautio, "A wideband array of stacked patch antennas using embedded air cavities in ltcc," *IEEE Microwave and Wireless Components Letters*, vol. 15, no. 12, pp. 916–918, Dec 2005.

[36] R. Garg, *Microstrip Antenna Design Handbook*, ser. Antennas and Propagation Library. Artech House, 2001. [Online]. Available: https://books.google.com/books?id=_er1LO5pEnUC

[37] D. Cassioli, L. A. Annoni, and S. Piersanti, "Characterization of path loss and delay spread of 60-ghz uwb channels vs. frequency," in *2013 IEEE International Conference on Communications (ICC)*, June 2013, pp. 5153–5157.

[38] A. Valdes-Garcia, S. Reynolds, A. Natarajan, D. Kam, D. Liu, J. W. Lai, Y. L. O. Huang, P. Y. Chen, M. D. Tsai, J. H. C. Zhan, S. Nicolson, and B. Floyd, "Single-element and phased-array transceiver chipsets for 60-ghz gb/s communications," *IEEE Communications Magazine*, vol. 49, no. 4, pp. 120–131, April 2011.

[39] S. Kishimoto, N. Orihashi, Y. Hamada, M. Ito, and K. Maruhashi, "A 60-ghz band cmos phased array transmitter utilizing compact baseband phase shifters," in *2009 IEEE Radio Frequency Integrated Circuits Symposium*, June 2009, pp. 215–218.

[40] A. Hajimiri, A. Komijani, A. Natarajan, R. Chunara, X. Guan, and H. Hashemi, "Phased array systems in silicon," *IEEE Communications Magazine*, vol. 42, no. 8, pp. 122–130, Aug 2004.

[41] W. L. Chan and J. R. Long, "A 60-ghz band 2 x 2 phased-array transmitter in 65-nm cmos," *IEEE Journal of Solid-State Circuits*, vol. 45, no. 12, pp. 2682–2695, Dec 2010.

[42] W. Menzel, D. Pilz, and M. Al-Tikriti, "Millimeter-wave folded reflector antennas with high gain, low loss, and low profile," *IEEE Antennas and Propagation Magazine*, vol. 44, no. 3, pp. 24–29, Jun 2002.

[43] Z. Li, H. Mopidevi, O. Kaynar, and B. A. Cetiner, "Beam-steering antenna based on parasitic layer," *Electronics Letters*, vol. 48, no. 2, pp. 59–60, January 2012.

[44] K. Deb, A. Pratap, S. Agarwal, and T. Meyarivan, "A fast and elitist multiobjective genetic algorithm: NSGA-II," *IEEE Transactions on Evolutionary Computation*, vol. 6, no. 2, pp. 182–197, 2002.

[45] D. M. Pozar, "Microstrip antennas," *Proceedings of the IEEE*, vol. 80, no. 1, pp. 79–91, Jan 1992.

[46] J. Kovitz and Y. Rahmat-Samii, "Using thick substrates and capacitive probe compensation to enhance the bandwidth of traditional cp patch antennas," *Antennas and Propagation, IEEE Transactions on*, vol. 62, no. 10, pp. 4970–4979, Oct 2014.

[47] B.-L. Ooi, S. Qin, and M.-S. Leong, "Novel design of broad-band stacked patch antenna," *Antennas and Propagation, IEEE Transactions on*, vol. 50, no. 10, pp. 1391–1395, Oct 2002.

[48] K. Tong, K. Li, T. Matsui, and M. Izutsu, "Broad-band double-layered coplanar patch antennas with adjustable cpw feeding structure," *Antennas and Propagation, IEEE Transactions on*, vol. 52, no. 11, pp. 3153–3156, Nov 2004.

[49] T. Seki, N. Honma, K. Nishikawa, and K. Tsunekawa, "A 60-ghz multilayer parasitic microstrip array antenna on ltcc substrate for system-on-package," *Microwave and Wireless Components Letters, IEEE*, vol. 15, no. 5, pp. 339–341, May 2005.

[50] R. J. Mailloux, *Phased Array Antenna Handbook*. Norwood, MA, USA: Artech House, 1994.

[51] D. Parker and D. C. Zimmermann, "Phased arrays - part 1: theory and architectures," *IEEE Transactions on Microwave Theory and Techniques*, vol. 50, no. 3, pp. 678–687, Mar 2002.

[52] ——, "Phased arrays-part ii: implementations, applications, and future trends," *IEEE Transactions on Microwave Theory and Techniques*, vol. 50, no. 3, pp. 688–698, Mar 2002.

[53] R. Harrington, "Reactively controlled directive arrays," *IEEE Transactions on Antennas and Propagation*, vol. 26, no. 3, pp. 390–395, May 1978.

[54] G. Breedi, "A review of rf/microwave switching technologies," *High Frequency Electronics*, 2010.

[55] K. Kohama, T. Ohgihara, and Y. Murakami, "High power dpdt antenna switch mmic for digital cellular systems," *IEEE Journal of Solid-State Circuits*, vol. 31, no. 10, pp. 1406–1411, Oct 1996.

[56] H. Takasu, F. Sasaki, H. Kawasaki, H. Tokuda, and S. Kamihashi, "W-band spst transistor switches," *IEEE Microwave and Guided Wave Letters*, vol. 6, no. 9, pp. 315–316, Sept 1996.

[57] D. A. Blackwell, D. E. Dawson, and D. C. Buck, "X-band mmic switch with 70 db isolation and 0.5 db insertion loss," in *Microwave and Millimeter-Wave Monolithic Circuits Symposium, 1995. Digest of Papers., IEEE 1995*, May 1995, pp. 97–100.

[58] Z. Li, E. Ahmed, A. M. Eltawil, and B. A. Cetiner, "A beam-steering reconfigurable antenna for wlan applications," *IEEE Transactions on Antennas and Propagation*, vol. 63, no. 1, pp. 24–32, Jan 2015.

[59] K. Nakayama, K. Kojima, F. Hayakawa, Y. Imai, A. Kitagawa, and M. Suzuki, "Submicron nonvolatile memory cell based on reversible phase transition in chalcogenide glasses," *Japanese Journal of Applied Physics*, vol. 39, no. 11R, p. 6157, 2000. [Online]. Available: http://stacks.iop.org/1347-4065/39/i=11R/a=6157

[60] S. Lai and T. Lowrey, "Oum - a 180 nm nonvolatile memory cell element technology for stand alone and embedded applications," in *Electron Devices Meeting, 2001. IEDM '01. Technical Digest. International*, Dec 2001, pp. 36.5.1–36.5.4.

[61] C. Peng, L. Cheng, and M. Mansuripur, "Experimental and theoretical investigations of laser-induced crystallization and amorphization in phase-change optical recording media," *Journal of Applied Physics*, vol. 82, no. 9, p. 4183, 1997. [Online]. Available: http://scitation.aip.org/content/aip/journal/jap/82/9/10.1063/1.366220

[62] D. A. Baker, M. A. Paesler, G. Lucovsky, S. C. Agarwal, and P. C. Taylor, "Application of bond constraint theory to the switchable optical memory material $ge_2sb_2te_5$," *Phys. Rev. Lett.*, vol. 96, p. 255501, Jun 2006. [Online]. Available: http://link.aps.org/doi/10.1103/PhysRevLett.96.255501

[63] A. Pergament, A. Crunteanu, A. Beaumont, G. Stefanovich, and A. Velichko, "Vanadium Dioxide: Metal-Insulator Transition, Electrical Switching and Oscillations. A Review of State of the Art and Recent Progress," jan 2016. [Online]. Available: http://arxiv.org/abs/1601.06246

[64] P. J. Hood and J. F. DeNatale, "Millimeter-wave dielectric properties of epitaxial vanadium dioxide thin films," *Journal of Applied Physics*, vol. 70, no. 1, p. 376, 1991. [Online]. Available: http://scitation.aip.org/content/aip/journal/jap/70/1/10.1063/1.350285

[65] J. SAKAI and M. KURISU, "Effect of pressure on the electric-field-induced resistance switching of VO2 planar-type junctions," *Physical review B. Condensed matter and materials physics*, vol. 78, no. 3. [Online]. Available: http://cat.inist.fr/?aModele=afficheN{&}cpsidt=20717580

[66] B. J. Kim, Y. W. Lee, S. Choi, S. J. Yun, and H. T. Kim, "VO_2 thin-film varistor based on metal-insulator transition," *IEEE Electron Device Letters*, vol. 31, no. 1, pp. 14–16, Jan 2010.

[67] G. Subramanyam, E. Shin, D. Brown, and H. Yue, "Thermally controlled vanadium dioxide thin film microwave devices," in *2013 IEEE 56th International Midwest Symposium on Circuits and Systems (MWSCAS)*, Aug 2013, pp. 73–76.

[68] Y. Zhou, X. Chen, C. Ko, Z. Yang, C. Mouli, and S. Ramanathan, "Voltage-triggered ultrafast phase transition in vanadium dioxide switches," *IEEE Electron Device Letters*, vol. 34, no. 2, pp. 220–222, Feb 2013.

CURRICULUM VITAE

Abdurazag Mohamad Khalat

Published Conference Papers

- A 60 GHz Beam-Steering Reconfigurable Antenna, A. Khalat; Md. A. Towfiq; O. Ceylan; and N. Biyikli; and B.A. Cetiner, in IEEE International Symposium on Antennas and Propagation, AP-S/URSI 2016.

- Broadband High-gain 60 GHz Antenna Array,Md. A. Towfiq; A. Khalat; O. Ceylan; and N. Biyikli, and B.A. Cetiner , in *IEEE International Symposium on Antennas and Propagation, AP-S/URSI* 2016.

- A low-cost reconfigurable mm-wave antenna, A. Khalat; Md. A. Towfiq; O. Ceylan; and N. Biyikli, B.A. Cetiner, in *In preparation, IEEE Trans. On Antennas and Propagation.*

- A new class of reconfigurable antenna m-wave array, A. Khalat; Md. A. Towfiq; O. Ceylan; and N. Biyikli; and B.A. Cetiner, in *preparation.*

- A mm-wave reconfigurable antenna array, A. Khalat; Md. A. Towfiq; O. Ceylan; and N. Biyikli; and B.A. Cetiner, in *preparation.*

- VO_2 based frequency reconfigurable antenna, A. Khalat; Md. A. Towfiq; O. Ceylan; and N. Biyikli, B.A. Cetiner, in *In preparation,TAP.*